Human-guided multi-robot cooperative manipulation

Dominik Sieber, *Student Member, IEEE,* and Sandra Hirche, *Senior Member, IEEE*

***Abstract*—The interaction of a human with a team of cooperative robots, which collaboratively manipulate an object, poses significant challenges for the control design. In this work we propose a formation-based approach to map the human input to the motion of the object cooperatively manipulated by multiple manipulators which feature local compliance control at the end-effector level. The formation-based approach guarantees that the reference trajectories maintain a desired geometry with respect to each other. Without being in touch with the object the human operator is part of the formation and guides the robots explicitly. Here the human can be interpreted as a leader in a leader-follower formation with the robotic manipulators being the followers. We analyze the system consisting of human operator and multi-robot manipulation task in both the transient phase and the steady-state for which we derive the equilibrium of the object pose from the human input and show its stability. A controllability analysis suggests that it is beneficial to make the state of the human accessible to all manipulators in order to reduce internal stress on the object. The proposed approach is evaluated in a full-scale multi-robot cooperative manipulation experiment with a human.**

***Index Terms*—Multi-robot systems, Human-robot interaction, Human-swarm interaction, Cooperative manipulation**

I. Introduction

WHILE the physical cooperation of several manipulators to achieve a common task has received some attention in recent years [1]–[3], the interaction between a team of physically cooperating robots and humans has been far less explored. The employment of human-guided cooperative manipulators covers application areas including collaborative assembly in manufacturing, construction, logistics, and search-and-rescue. For manipulation tasks the cooperation of two or more partners is often crucial to enhance functionality and flexibility. This setting of multiple robots guided by a human is particularly attractive as the multi-robot team typically outperforms the human at repetitive and physically exhausting tasks but not at cognitive reasoning in unstructured environments. On the contrary, humans are very skilled in reasoning and decision making even in previously unknown situations. Therefore some attention has been dedicated to problem settings where a human acts as an operator of an automated complex system [4]. Largely unexplored question is how the human command should be mapped into the action space of the robots in a cooperative manipulation task which is the topic of this article.

In this article we investigate the prototypical task where a human operator controls a multi-robot cooperative manipulation task. We present a control scheme for a human to guide several robotic manipulators which cooperatively manipulate an object to a final configuration. In a cooperative manipulation task it is essential that there is no significant deviation of the forces exerted on the manipulated object from the desired forces. Model uncertainties are always present and can be considered by rendering each manipulator compliant with an impedance control scheme in order to avoid high internal stress acting on the object. Particular set-points for each cooperating robot need to be generated which respect the kinematic coordination of the robots' motion and the human command. We formulate the coordination problem as a formation control framework in which set-points are distributedly generated for the robotic manipulators. The human operator is considered as the leader of the formation and controls the set-points of the particular robots with the movement of his/her hand.

The contribution of this article is a novel approach for the human guidance of a multi-robot cooperative manipulation task. It is based on a leader-follower formation control approach. We discuss system equilibria and their stability and show that the human-guided set-point generator and the impedance-based multi-robot interaction dynamics are asymptotically stable for a human pose command being the input. Particularly critical for the occurrence of internal forces is also the transient phase, where excessive forces can easily occur if the motion transients of the individual robots do not match. We approach this issue by a controllability analysis of the human-robot team interaction in cooperative manipulation. In particular, we investigate the controllable eigenmodes of the robot formation. We show that it is beneficial in terms of the reduction of undesired internal forces during the transient phase if every robot has direct access to the state information of the human leader. Based on these results we devise a control strategy for human-controlled formations of physically cooperating robots.

A. Related work

The design of interaction mechanisms to efficiently guide multiple robots is a very recent topic and only a limited amount of work is available in the literature. Controlling multiple robots is explored in multi-robot teleoperation [5] where a group of slave robots is controlled by the human. However the actual task of manipulating an object is only incorporated by grasping shape function [6] without considering the interaction dynamics. Similarly, the interaction of a human with a swarm of robots as in [7] does not account for physical coupling among the robotic agents. The forward mapping from human to robots is designed to satisfy robotic state constraints where the human influence is evaluated by a controllability analysis [8]. In case of non-holonomic mobile robots additionally input constraints need to be considered [9]. The responsibility of adhering to

Manuscript received August XX, 20XX; revised August XX, 20XX; accepted November XX, 20XX. The work is partly supported by the European Union Seventh Framework Programme FP7/2007-2013 within the ERC Starting Grant Control based on Human Models (con-humo), grant agreement no. 337654, partly under grant agreement no. 601165 of the project "WEARHAP - Wearable Haptics for Humans and Robots".

Both authors are with the Chair of Information-Oriented Control, Department of Electrical Engineering and Information Technology, Technische Universität München, D-80290 Munich, Germany. (e-mail: {dominik.sieber, hirche}@tum.de)

these input constraints is with the human: constraint violation is signaled to the human via visuo-haptic information [10]. Common input technologies for guiding the loosely coupled multi-robot system are mobile handhelds [11] or gesture-based interfaces [12]. A haptic interaction method for swarms can improve the user experience by an optimal interaction location [13]. All these works consider the interaction of a user with a group of robots but lack the physical coupling through the object with state and input constraints as in cooperative robotic manipulation [14]. Hence, it remains open whether and how we can transfer the stability and controllability properties to the physically cooperating manipulators.

The approaches mentioned above do not discuss a uniform forward mapping, i.e. if the operator should directly control the robot positions (*position control*) or the velocities (*rate control*). We employ position control based on multi-agent formation control. For teleoperation in robotics [15] position control usually outperforms rate control. Furthermore, in position control the drawbacks of differential approaches are avoided as error accumulation [16]. Since the coordination of multiple robots relies on the differential kinematics between object and manipulators through the grasp matrix [17], a position control scheme can only be applied with a proper mechanism such as a formation-based approach with potential fields [18]. Formation control for cooperative mobile robot manipulation is explored under the term caging for example in [19]. To compensate for formation uncertainties in cooperative manipulation a distributed impedance-based control scheme is employed in [20], which controls the internal forces [21].

A preliminary version of this work appeared in [22]. In this article we provide an additional analysis of the internal forces based on the translational and nonlinear rotational dynamics of object and multiple robots and the 6 DoF set-point generator. Furthermore, a weighted set-point generation is proposed which avoids undesired forces and the system stability is shown.

The remainder of this article is organized as follows. Section II describes formally the dynamical system of physically cooperating robots. In Section IV the resulting internal stress in a formation-based set-point generator is discussed. Stability is analyzed in Section III and controllability is discussed in Section V. The experimental evaluation is presented in VI.

II. Cooperative manipulation task

In this work we consider a human-robot interaction task where multiple manipulators rigidly grasp an object. The rigidly grasped object is effortlessly manipulated by a single human through the movement of his/her hand by guiding the set-points of the cooperating robots. The general setup with physically cooperating manipulators is depicted in Fig. 1. The objective of the human is to guide a cooperatively manipulated object starting from an initial configuration to a goal configuration. In this setup autonomous functionalities such as avoidance of excessive forces on the object or obstacle avoidance are required to be masked from the human operator. To achieve this we employ an interaction mechanism which establishes a formation to generate the individual desired robot trajectories such that all robots move in compliance with the object geometry and only the desired force are exerted on the manipulated object by the manipulators. For the description of the overall system dynamics, a virtual coordinate system is attached to each end-effector denoted by Σ_i and to the manipulated object denoted by Σ_o. For the sake of exposition let the coordinate systems Σ_i and Σ_o be aligned in the world frame Σ_w as $R_o^i = I_3$, where R_o^i is a rotation matrix from end-effector frame Σ_i to object frame Σ_o.

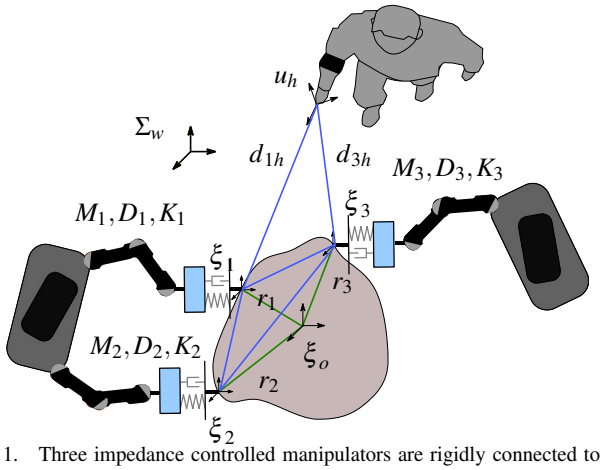

Fig. 1. Three impedance controlled manipulators are rigidly connected to the object. To control the desired internal forces acting on the object the set-points of the mass-spring-damper systems are driven by a formation-based control approach.

A. Manipulator and object dynamcics

The equations of motion of the manipulated object and of the impedance-controlled robotic manipulators are outlined in this section. In order to allow minor deviations of the desired position trajectories from the constraints, which can result e.g. from model and geometric uncertainties or external disturbances, we employ a impedance control scheme for each of the N manipulators here. The Cartesian impedance control [23] for each manipulator is described as

$$M_i \dot{v}_i + D_i v_i + h_i^{\mathscr{K}}(\xi_i, \xi_i^d) = h_i - h_i^d \tag{1}$$

where $\xi_i = [p_i^\mathsf{T}, q_i^\mathsf{T}]$ denotes the pose and $h_i = [f_i^\mathsf{T}, t_i^\mathsf{T}]^\mathsf{T} \in \mathbb{R}^3$ is the applied wrench to the i-th manipulator. Here, the pose is split into the end-effector position $p_i \in \mathbb{R}^3$ describing the translational part and the unit quaternion $q_i = (\eta_i, \varepsilon_i)^\mathsf{T} \in SO(3)$ describing the rotational part where $\eta_i \in \mathbb{R}$ is the real part and $\varepsilon_i \in \mathbb{R}^3$ is the imaginary part. Throughout this article all quaternions q_i are unit quaternions i.e. $q_i^\mathsf{T} q_i = 1$. In line with the literature the twist v_i is defined by the end-effector's translational and angular velocity as $v_i = \left[\dot{p}_i^\mathsf{T}, \omega_i^\mathsf{T}\right]^\mathsf{T} \in \mathbb{R}^6$. A proper conversion between the time derivative of the robot state $\dot{\xi}_i$ and the twist v_i is given by

$$v_i = \begin{bmatrix} I_3 & 0 \\ 0 & 2U(q_i)^\mathsf{T} \end{bmatrix} \dot{\xi}_i, \tag{2}$$

where the conversion can be compactly written with the help of an aid matrix $U(q_i) \in \mathbb{R}^{4\times 3}$ defined as

$$U(q_i) = \begin{pmatrix} -\varepsilon_i^\mathsf{T} \\ \eta_i I_3 + S(\varepsilon_i) \end{pmatrix}. \tag{3}$$

Here, the operator $S(\cdot)$ is the skew-symmetric matrix operator defining the cross product, i.e. $S(a)b = a \times b$. For unit quaternions the aid matrix $U(q_i)$ features the following identities

$$U(q_i)U(q_i)^\intercal = I_4 - q_i q_i^\intercal \text{ and} \tag{4a}$$
$$U(q_i)^\intercal q_i = 0. \tag{4b}$$

The wrench h_i is split into forces and torques $f_i, t_i \in \mathbb{R}^3$. Furthermore, the desired manipulator pose is represented by $\xi_i^d = [p_i^d, q_i^d]$ and the desired wrench by h_i^d. Here, $p_i^d \in \mathbb{R}^3$ is the desired position and $q_i^d = \left[\eta_i^d, \varepsilon_i^d\right] \in \mathbb{S}^3$ is the desired orientation where ν_i^d is the scalar part and ε_i^d is the vector part of the quaternion. The compliance is represented by $M_i = \text{diag}(m_i I_3, \mu_i I_3), D_i = \text{diag}(d_i I_3, \delta_i I_3), K_i = \text{diag}(k_i I_3, \kappa_i I_3) \in \mathbb{R}^{6\times 6}$ which are the positive definite mass, damping, and stiffness matrices, respectively. The translational behavior is determined by scalar values $m_i, d_i, k_i \in \mathbb{R}^+$ rendering an isotropic translational behavior. The rotational behavior is specified by the scalar parameters $\mu_i, \tau_i, \kappa_i \in \mathbb{R}^+$. A stiffness in six degrees-of-freedom is given by

$$h_i^{\mathscr{K}}(\xi_i, \xi_i^d) = \begin{bmatrix} f_i^K \\ t_i^\kappa \end{bmatrix} = \begin{bmatrix} k_i(p_i - p_i^d) \\ 2\kappa_i U(q_i)^\intercal (q_i - q_i^d) \end{bmatrix}, \tag{5}$$

where the force f_i^K is defined as the product between the translational error and the corresponding stiffness value k_i. The rotational error between the current and the desired orientation is defined as the imaginary part of the quaternion product $q_i \cdot (q_i^d)^{-1}$ and can be expressed with (3) as $U(q_i)^\intercal (q_i - q_i^d)$. The applied torque t_i^κ is the product between rotational error and the stiffness value κ_i. In case of a free-space motion, i.e. $h_i = 0$ and no desired wrench $h_i^d = 0$, it is straightforward using Lyapunov theory [24] to show that the set-point converges as

$$\lim_{t\to\infty} \xi_i = \xi_i^d. \tag{6}$$

Note that the robotic manipulators can still have different dynamics and hardware restrictions. By designing appropriate nonlinear feedback control law similar to [23] the apparent dynamics of the robot can be expressed as (1). Hence, the applied wrench to the environment, that is in our case the object, does not explicitly depend on different robot dynamics but it does only depend on the tuneable impedance parameters M_i, D_i, K_i. For simplicity of exposition we want to avoid effects which arise from heterogenous or non-isotropic impedance parameters.

Assumption 1: The impedance parameters are isotropic in all dimensions and for all manipulators, i.e. $m = m_i, d = d_i, k = k_i, \mu = \mu_i, \delta = \delta_i, \kappa = \kappa_i \forall i$

The equation of motion of the object is given by

$$M_o \dot{v}_o + \begin{bmatrix} 0 & 0 \\ 0 & S(\omega_o) J_o \end{bmatrix} v_o + \begin{bmatrix} -m_o g \\ 0 \end{bmatrix} = h_o, \tag{7}$$

where h_o is the effective wrench acting on the object resulting from the interaction with in our case the manipulators or generally the environment. $M_o = \text{diag}(m_o I_3, J_o)$ and $m_o \in \mathbb{R}^+$ is the mass and $J_o \in \mathbb{R}^{3\times 3}$ is the inertia of the object. The gravity vector is denoted by g. Furthermore, $\xi_o = \left[p_o^\intercal, q_o^\intercal\right]$ and $v_o = \left[\dot{p}_o^\intercal, \omega_o^\intercal\right]^\intercal$ is the object pose and twist, respectively. For illustration we build up simple examples for the setup which is employed in the experiments.

Example 1: Let us consider robot dynamics (1) along one translational dimension. We choose the scalar damping to be $d_i = 120$, the stiffness to be $k_i = 160$, the mass to be $m_i = 10$, and $f_i^d = 0$ yielding

$$10\ddot{p}_i + 120\dot{p}_i + 160 p_i = 160 p_i^d + f_i. \tag{8}$$

The initial position is $p_i(t_0) = 0$ and at $t = 1s$ the desired position p_i^d of each robot is set to 1. Between $t = 5s$ and $t = 7s$ an external force $f_i = -20N$ acts on the manipulator which causes a deviation of the robot trajectory from the desired position p_i^d as depicted in Fig. 2.

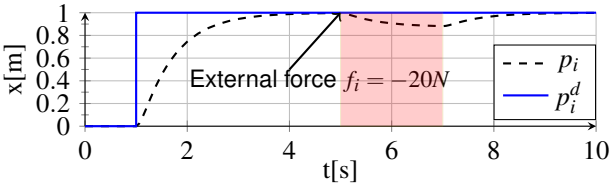

Fig. 2. Robot trajectories p_i resulting from step response at $t = 1s$. Deviation of the trajectory from the desired position results from an external force $f_i = -20N$ between $t = 5s$ and $t = 7s$.

B. Kinematic constraints in cooperative manipulation

In a cooperative manipulation task as depicted in Fig. 1 the object and manipulators cannot move independently of each other, i.e. all motions are coupled and there are constraints between the motion of the object and of the manipulators which are now presented. We consider a cooperative manipulation task where the manipulated object is rigid and the robotic end-effectors are rigidly connected to the object. Due to that we can express the position p_i of the ith robot as a function of the distance to the object center and the quaternion q_i as

$$\xi_i = \begin{bmatrix} p_i \\ q_i \end{bmatrix} = \begin{bmatrix} p_o + r_i \\ q_o \end{bmatrix} \tag{9}$$

where the displacement $r_i = R_o(q_o)^o r_i$ indicates the relative displacement between the object frame and the end-effector frame and $R_o(q_o) \in \mathbb{R}^{3\times 3}$ is a rotation matrix from world frame to object frame. Rigidly connected end-effectors yield a constant displacement in the object frame as ${}^o r_i = \text{const}$.

Assumption 2: We assume the object frame Σ_o is in the geometric center of all manipulator frames Σ_i.
This assumption does not pose any restriction and is merely for the convenience of representation as it implies the following equality condition for the relative displacements

$$\sum_i {}^o r_i = \sum_i r_i = 0. \tag{10}$$

The constraints of a cooperation manipulation task (9) are differentiated w.r.t. time as

$$v_i = \begin{bmatrix} \dot{p}_i \\ \omega_i \end{bmatrix} = \begin{bmatrix} \dot{p}_o + S(r_i)^\intercal \omega_o \\ \omega_o \end{bmatrix} = G_i(r_i)^\intercal v_o, \tag{11}$$
$$\dot{v}_i = \begin{bmatrix} \ddot{p}_i \\ \dot{\omega}_i \end{bmatrix} = \begin{bmatrix} \ddot{p}_o + S(r_i)^\intercal \omega_o + S(\omega_o)^2 r_i \\ \dot{\omega}_o \end{bmatrix}, \tag{12}$$

where the matrix $G_i(r_i) \in \mathbb{R}^{6\times 6}$ is a submatrix of the grasp matrix $G \in \mathbb{R}^{6\times 6N}$ which is defined by

$$G = [G_1, G_2, \ldots, G_N] \text{ where } G_i = \begin{bmatrix} I_3 & 0 \\ S(r_i) & I_3 \end{bmatrix}. \tag{13}$$

We are now ready to compactly rewrite the constrained acceleration condition (12) for all manipulators i as

$$A \begin{bmatrix} \dot{v}_o \\ \dot{v} \end{bmatrix} = b, \tag{14}$$

where $\dot{v} = \left[\dot{v}_1^\intercal, \ldots, \dot{v}_N^\intercal\right]^\intercal \in \mathbb{R}^{6N}$ are the concatenated accelerations of the manipulator states. The constraint matrix $A \in \mathbb{R}^{6N \times 6(N+1)}$ and the centripetal terms $b \in \mathbb{R}^{6N}$ are then

$$A = \begin{bmatrix} -G^\intercal & I_{6N} \end{bmatrix} \text{ and } b = \begin{bmatrix} S(\omega_o)^2 r_1 \\ 0 \\ \cdot \\ S(\omega_o)^2 r_N \\ 0 \end{bmatrix}, \tag{15}$$

which represents the constraints of object and manipulators.

C. Constrained dynamics of multiple manipulators and object

So far the dynamics of object and manipulators are considered separately in Sec. II-C and are linked together by the constraints of cooperative manipulation in Sec. II-B. In this section both dynamics (1), (7) and constraints (14) are combined into a single dynamical system by deriving a joint system model of object and impedance controlled manipulators which is driven by distributed set-points. The inputs of the manipulators dynamics (1) and the object dynamics (7), respectively and are given by

$$h_o^\Sigma = -\begin{bmatrix} 0 & 0 \\ 0 & S(\omega_o)J_o \end{bmatrix} v_o - \begin{bmatrix} -m_o g \\ 0 \end{bmatrix} \text{ and} \tag{16}$$

$$h_i^\Sigma = -D_i v_i - h_i^{\mathscr{K}}(\xi_i, \xi_i^d) - h_i^d. \tag{17}$$

By applying the Gauss' principle of least constraint for the constrained motion of multiple dynamics [25] a linear projection indicates to what extent the particular input wrenches $h^\Sigma = \left[h_1^\Sigma, \ldots, h_N^\Sigma\right] \in \mathbb{R}^{6N}$ and $h_o^\Sigma \in \mathbb{R}^6$ of the dynamics (1) and (7) satisfy the constraint (14):

$$\begin{bmatrix} h_o \\ h \end{bmatrix} = A^\intercal \left(A\bar{M}^{-1}A^\intercal\right)^{-1} \left(b - A\bar{M}^{-1} \begin{bmatrix} h_o^\Sigma \\ h^\Sigma \end{bmatrix}\right), \tag{18}$$

where $\bar{M} = \operatorname{diag}(M_o, M_1, \ldots, M_N)$ is a block-diagonal matrix of all mass matrices. Let now be $M = \operatorname{diag}(M_1, \ldots, M_N)$. By employing (15) into (18) the interaction wrench h_o of the object is given by

$$h_o = -GQG^\intercal M_o^{-1} h_o^\Sigma + GQM^{-1}h^\Sigma - GQb, \tag{19}$$

where we additionally introduce the auxiliary matrix $Q = (M^{-1} + G^\intercal M_o^{-1} G)^{-1}$ for reasons of better readability. We are now ready to model the system dynamics of multiple manipulators and object by replacing h_o and h_o^Σ in (7):

$$M_o \dot{v}_o = (I_6 - GQG^\intercal M_o^{-1}) h_o^\Sigma + GQM^{-1}h^\Sigma - GQb. \tag{20}$$

After application of Woodbury and Searle matrix identities the object dynamics (20) can be expressed as

$$(M_o + \sum G_i M_i G_i^\intercal)\dot{v}_o = h_o^\Sigma + \sum_i G_i h_i^\Sigma - GMb. \tag{21}$$

Finally, we substitute (15), (16), and (17) in (21). Here, we set $\sum_i G_i h_i^d = [-m_o g^\intercal, 0^\intercal]^\intercal$ to account for the object's gravity force and the overall dynamics is given by

$$\mathscr{M}\dot{v}_o + \mathscr{D}v_o + \mathscr{C}_o v_o + \mathscr{K}_o \xi_o = \sum_i \mathscr{K}_i \xi_i^d + \tilde{h}_o, \tag{22}$$

where $\tilde{h}_o$ is an external disturbance and the apparent inertia $\mathscr{M}$, damping $\mathscr{D}$, coriolis-centripetal matrix $\mathscr{C}_o$, and the stiffness $\mathscr{K}_o, \mathscr{K}_i$ result in

$$\mathscr{M} = \begin{bmatrix} (m_o + \sum m_i) I_3 & 0 \\ 0 & J_o + \sum \mu_i I_3 + m_i S(r_i) S(r_i)^\intercal \end{bmatrix},$$

$$\mathscr{D} = \begin{bmatrix} \sum_i d_i I_3 & 0 \\ 0 & \sum \delta_i + d_i S(r_i) S(r_i)^\intercal \end{bmatrix},$$

$$\mathscr{C}_o = \begin{bmatrix} 0 & \sum m_i S(\omega_o) S(r_i)^\intercal \\ 0 & S(\omega_o) J_o + \sum m_i S(r_i) S(\omega_o) S(r_i)^\intercal \end{bmatrix},$$

$$\mathscr{K}_o = \begin{bmatrix} \sum_i k_i I_3 & 0 \\ 0 & \sum_i \kappa_i U(q_o)^\intercal \end{bmatrix} \text{ and}$$

$$\mathscr{K}_i = \begin{bmatrix} k_i I_3 & 0 \\ k_i S(r_i) & \kappa_i U(q_o)^\intercal \end{bmatrix}.$$

Here, the off-diagonal entries $\sum m_i S(r_i)^\intercal, \sum m_i S(r_i)$ in $\mathscr{M}$, $\sum_i d_i S(r_i), \sum d_i S(r_i)^\intercal$ in $\mathscr{D}$, and $k_i S(r_i)^\intercal$ in $\mathscr{K}_o$ vanish due to Assumptions 1 and 2. For a more detailed derivation and analysis of this interaction model the reader is referred to [14]. Note that for the equation of motion (22) we obtain a centralized equation of motion for ξ_o which is driven by decentralized set-point inputs $\mathscr{K}_i \xi_i^d$ from each attached manipulator.

D. Internal force as formation-maintaining forces

The manipulators and the object are physically coupled. At the same time however, the desired pose for the manipulators can be set independently of each other. These reference inputs may violate the kinematic constraints and result in internal forces which do not induce a motion of object and manipulators. Internal forces can be interpreted as formation-maintaining forces. We derive the formulation for internal forces by shifting the reference into one particular agent i, denoted by p_i, which is the reference for all the others, denoted by p_j. Employing (9) between any pair i and j the desired displacement d_{ij} is given by

$$p_i - p_j = d_{ij} = r_i - r_j, \tag{23}$$

for which the rotation of the object $R_o(q_o)$ is required in the world frame. The rotational constraint between two frames i and j can be expressed using quaternion formalism as follows

$$q_i = q_j. \tag{24}$$

For the sake of exposition let now be $i = 1$ and $j = 2, \ldots, N$. Derivating (23) and (24) twice w.r.t time yields a modified constraint matrix

$$\bar{A} = \begin{bmatrix} -G^\intercal(d_1) & I_{6(N-1)} \end{bmatrix} \text{ and } \bar{b} = \begin{bmatrix} S(\omega_o)^2 d_{12} \\ 0 \\ \vdots \\ S(\omega_o)^2 d_{1N} \\ 0 \end{bmatrix},$$

where $d_1 = [d_{12}, \ldots, d_{1N}]$. An explicit solution for the internal force h^{int} is given by [14]

$$h^{\text{int}} = M^{\frac{1}{2}} (\bar{A} M^{-\frac{1}{2}})^\dagger (\bar{b} - \bar{A} M^{-1} h^\Sigma). \tag{25}$$

Note here that the desired set-points need to be generated for each physically cooperating robot. Hence, decentralized inputs ξ_i^d can cause an violation of the constraint (23) and (24) and can thus result in an internal force.

Remark 1: Note that isotropic and homogenous impedance parameters do not result in internal forces from the system dynamics. In fact, it is straightforward to show with (25) that the system dynamics do not induce an internal force if the natural frequency $\omega_i = \sqrt{\frac{k_i}{m_i}}$ and the damping ratio $\zeta_i = \frac{d_i}{2\sqrt{k_i m_i}}$ are equal for each robot, i.e. $\omega_i = \omega_j, \zeta_i = \zeta_j, \forall (i,j)$. Other parametrisation result in undesired internal forces during the transient phase which is excluded here by Assumption 1.

In this work we set the desired internal force to zero in order to simplify the argumentation. However, the principle approach also holds for non-zero internal force. At this stage we are interested how the set-points ξ^d need to be generated by a formation-based approach such that there is no internal force $h^{\text{int}} = 0$.

Hence, we neglect the effect of the desired forces and the motion, i.e. $h_i^d = v_i = v_0 = 0$. Consequently, $b = 0$ and the internal forces h^{int} (25) generated by distributed set-points (5) are given by

$$h^{\text{int}} = M^{\frac{1}{2}} (\bar{A} M^{-\frac{1}{2}})^{\dagger} \bar{A} M^{-1} \begin{bmatrix} k(p_1 - p_1^d) \\ -2\kappa U(q_1)^{\mathsf{T}} q_1^d \\ \vdots \\ k(p_N - p_N^d) \\ -2\kappa U(q_N)^{\mathsf{T}} q_N^d \end{bmatrix}. \tag{26}$$

Evaluating exemplarily the first equations of $\bar{A} M^{-1} h^{\Sigma}$ in (26) yields

$$\begin{aligned} f_1^{\text{int}} &= -k(p_1 - p_1^d) - S(d_{12}) 2\kappa U(q_1)^{\mathsf{T}} q_1^d + k(p_2 - p_2^d) \\ \tau_1^{\text{int}} &= 2\kappa U(q_1)^{\mathsf{T}} q_1^d - 2\kappa U(q_2)^{\mathsf{T}} q_2^d. \end{aligned}$$

Since $U(q_1)^{\mathsf{T}} = U(q_2)^{\mathsf{T}}$ due to (24) it is obvious that the internal torque $\tau_1^{\text{int}} = 0$ only if the rotations match $q_1^d = q_2^d$. For the internal force we have $f_1^{\text{int}} = 0$ if the current orientation q_1 matches the desired one as $q_1 = q_1^d$ and if $p_1^d - p_2^d = d_{12}$. For the latter result we employed (23) for the current set-points p_1, p_2. This result also holds for any manipulator pair i and j. In conclusion the desired property of the trajectory generator is to always satisfy the constraints (23) and (24) concerning the manipulator positions p_i, p_j and orientations q_i, q_j also for the desired set-point pair p_i^d, p_j^d and q_i^d, q_j^d as follows

$$p_i^d - p_j^d = d_{ij}. \tag{27}$$

$$q_i^d = q_j^d. \tag{28}$$

A special case is present when only translational motions are considered and the constraint matrix is then given by

$$\bar{\bar{A}} = \begin{bmatrix} 1 & I_{3(N-1)} \end{bmatrix}. \tag{29}$$

Under Assumption 1 a more specific result for the internal forces (25) is given by

$$f^{\text{int}} = (\sqrt{m})^2 \bar{\bar{A}}^{\dagger} \bar{\bar{A}} \frac{1}{m} k(p - p^d) = k \bar{\bar{A}}^{\dagger} \bar{\bar{A}} e, \tag{30}$$

where $e = p - p^d$, $p = [p_1^{\mathsf{T}}, \ldots, p_N^{\mathsf{T}}]^{\mathsf{T}} \in \mathbb{R}^{3N}$, and $p^d = [p_1^{d\mathsf{T}}, \ldots, p_N^{d\mathsf{T}}]^{\mathsf{T}} \in \mathbb{R}^{3N}$. Furthermore, $\bar{\bar{A}}^{\dagger} \bar{\bar{A}} \in \mathbb{R}^{3N \times 3N}$ reads as

$$\bar{\bar{A}}^{\dagger} \bar{\bar{A}} = I_N - \frac{1}{N} 1 1^{\mathsf{T}}. \tag{31}$$

By employing the average of the particular state $\bar{e} = \frac{1}{N}[\sum e_i^{\mathsf{T}}, \sum e_i^{\mathsf{T}}, \ldots, \sum e_i^{\mathsf{T}}]^{\mathsf{T}}$ we can simplify (30) as

$$f^{\text{int}} = k(e - \bar{e}). \tag{32}$$

The interpretation of (32) is that an internal force, $f^{\text{int}} \neq 0$, acts on the object if the particular robot inputs e are not equal to the averaged system input $\bar{e}$: $e \neq \bar{e}$. As a result an internal force $f^{\text{int}} \neq 0$ acts on the object. Hence, to avoid an internal force, $f^{\text{int}} = 0$, all inputs e need to be equal: $e_i = e_j = \frac{1}{N} \sum e_i$. We now want to illustrate the occurrence of internal forces based on the previous example.

Example 2: We continue here with the previously defined Example 1. An object is manipulated by three manipulators whose dynamics are defined in (8). The mass of object is $m_o = 1$ and the initial position is $p_o(t_0) = 0$. The particular manipulator dynamics (8) yield an overall dynamics given by

$$31\ddot{p}_o + 360\dot{p}_o + 480 p_o = \sum_{i=1}^{3} 160 p_i^d + \tilde{f}_o. \tag{33}$$

At $t = 1s$ the set-points are driven from $p^d = [0,0,0]^{\mathsf{T}}$ to $p^d = [0.9, 1, 1.1]^{\mathsf{T}}$. The motion of the object follows the desired position 0 to $\bar{p}^d = 1$, yet there is an internal force (32) as acting on the object as depicted in Fig 3. The reason for the internal force is a deviation of the particular desired positions p_1^d, p_3^d from p_2^d without satisfying the object geometry.

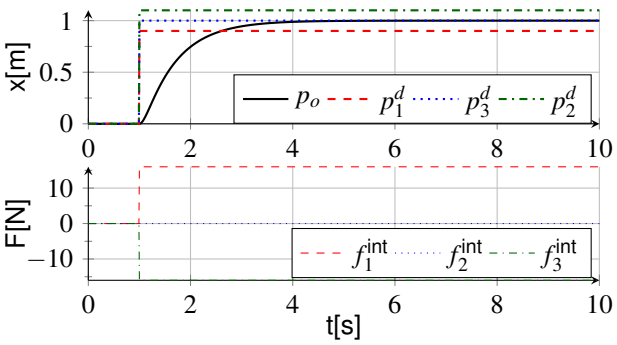

Fig. 3. Object trajectory p_o resulting from distributed robot set-points p_1^d, p_3^d, p_2^d. Deviation of the set-points results in an internal force $f_i^{\text{int}} \neq 0$.

After discussing internal forces in cooperative manipulation, we present a set-point generator to avoid internal forces.

E. General set-point generator to satisfy kinematic constraints

The motion and accordingly the desired poses $\xi_i^d = [p_i^{d\mathsf{T}}, q_i^{d\mathsf{T}}]^{\mathsf{T}}$ for each manipulator need to be in compliance with the object geometry to avoid internal forces as discussed before. We now present a uniform approach with which suitable set-points can be generated based on a formation control approach. We consider the desired position p_i^d and the desired orientation q_i^d for the ith end-effector being the state of a formation control approach which evolves according to

$$\dot{p}_i^d = u_i, \tag{34}$$

$$\dot{q}_i^d = \frac{1}{2} U(q_i^d) \omega_i, \tag{35}$$

where $u_i \in \mathbb{R}^3$ is the translational system input. Here, $\frac{1}{2} U(q_i^d) \omega_i$ is the quaternion propagation as e.g. defined in [26] where the angular input is given by ω_i. Note here that during translational

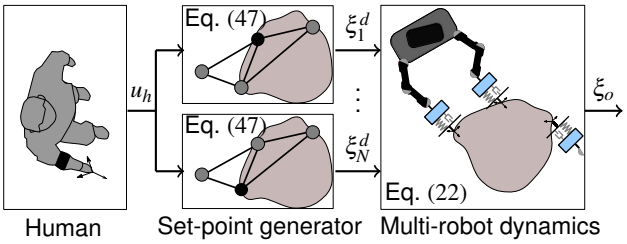

Fig. 4. General control approach for the cooperative manipulation task guided by the human input u_h. The human input u_h clearly determines the desired poses ξ^d of impedance-controlled manipulators and influences the actual pose ξ_o of the cooperatively manipulated object.

motions of each manipulator, the dynamics $\dot{p}^d_{i,k} = u_{i,k}$ for each translational degree of freedom $k \in \{1,2,3\}$ are decoupled. Using (27) a translational error for the set-point of the ith manipulator w.r.t the jth manipulator is defined as

$$e^p_{ij} = p^d_i - p^d_j - d_{ij}. \tag{36}$$

This formation is presented by a desired displacement $d_{ij} = [d_{ij,1}, d_{ij,2}, d_{ij,3}]$ among the cooperating manipulators i and j, which needs to be established and maintained throughout the complete task execution. Furthermore, the desired displacements d_{ij} have to be chosen to be *realizable* [27], i.e. there exist a $p^{d^*} = [p^{d^*}_1, \ldots, p^{d^*}_N] \in \mathbb{R}^{3N}$ such that $p^*_i - p^*_j = d_{ij},\ \forall (i,j)$. Note that the displacements are realizable when choosing them according to (27). Likewise the translational error (36) a suitable orientation error for the unit quaternion representing the ith manipulator is given by

$$e^o_{ij} = \eta^d_j \varepsilon^d_i - \eta^d_i \varepsilon^d_j - \varepsilon^d_i \times \varepsilon^d_j = -U(q^d_i)^\intercal q^d_j. \tag{37}$$

To minimize the translational error e^p_{ij} and the rotational error e^o_{ij} which is present between set-point i and any neighbor j we choose the input u_i of the translational movements to be $u_i = \sum_{j \in N_i} e^p_{ij}$ and the input ω_i of the rotational movements to be $\omega_i = \sum_{j \in N_i} e^o_{ij}$ Hence, a 6 DoF set-point generator is given by

$$\dot{p}^d_i = -\sum_{j \in N_i} e^p_{ij} + S(\tau_i) e^o_{ij}, \tag{38}$$

$$\dot{q}^d_i = -\sum_{j \in N_i} \frac{1}{2} U(q^d_i) e^o_{ij}, \tag{39}$$

where $S(\tau_i)e^o_{ij}$ is the radial motion which is present for two set-points on a rigid body during a rotational motion. Note here that the displacement vector τ_i determines the center of rotation. The desired displacement d_{ij} between i and j is transformed in the frame Σ_o as defined in (23). N_i describes the neighbors of agent i. In the following the set of neighborhood sets $\{N_1, \ldots, N_N\}$ is called interaction topology. Note that from a formation-control perspective, this approach is characterized as a displacement-based control approach [28] where the particular robots have to communicate the relative positions to their neighbors. Under the control law (38) the desired robot position converge to the desired formation if the underlying interaction topology resulting from the N_is is connected or if there exists a spanning tree [28] which we address in the following assumption.

Assumption 3: The interaction graph describing the interaction topology is undirected and connected.

Note here that the dynamical system (39) which determines the desired rotation $\dot{q}^d_i$ only depends on the rotational error e^o_{ij}. The dynamics of the translational set-point $\dot{p}^d_i$ depend on the translational error e^p_{ij} itself but additionally they are influenced by the rotational part e^o_{ij} due to the radial motion of the physically connected robots. Furthermore, we point out at this stage that the dynamics (38) and (39) do not guarantee collision avoidance [28] of the desired set-points among the manipulators. This is acceptable as a collision of two set-points results in no actual collision of the manipulators due to the rigid grasp. However, it violates the constraint (27) and therefore results in a corresponding internal force.

F. Compact formulation of human guidance

The objective of this work is to let the human operator to manipulate the object by being an active member of the formation without being physically in touch with the object as depicted in Fig. 1. Due to the generality of the formation-based approach the human operator can be easily integrated into the formation-based set-point generator as leading agent. To achieve this the desired displacements d_{ih} between the human and particular robots i have to be defined such that the virtual formation remains realizable. Therefore, the Cartesian pose $u_h = \left[x_h^\intercal, q_h^\intercal\right]^\intercal \in \mathbb{R}^7$ of the human is required in the world frame Σ_w. In our task x_h is the position and q_h is the orientation of the human hand which can e.g. be sensed by the robots.

Remark 2: In this work we focus on a direct and explicit interaction method where a human operator controls the robots non-physically by hand motion. Here, the hand motion is only one possible option for a direct interaction method. Alternatively, the command can be specified remotely by an appropriate input device as e.g. presented in [11]. The remaining results of this article still hold for such cases.

For a compact formulation of the human-guided set-point system model we transform the distributed set-points p^d_i into a particular reference. We choose this reference to be the center of rotation and transform the ith robot state as

$$x_i = \begin{bmatrix} x^p_i \\ x^q_i \end{bmatrix} = \begin{bmatrix} p^d_i - \tau_i \\ q^d_i \end{bmatrix}, \tag{40}$$

where τ_i is a displacement vector which satisfies $d_{ij} = \tau_i - \tau_j$. For the sake of exposition we choose the constant displacement of the human input used in the transformation (40) to be $\tau_h = 0$ which makes the human hand to be the center of rotation and

$$\tau_i = d_{ih}. \tag{41}$$

Remark 3: The strength of the human is to know the high-level task of indicating the object pose while the physical manipulation task is performed by multiple robots. If the human interfaces the robots through another device as discussed in Remark 2 it might be beneficial to change the center of rotation to be e.g. the center of mass, i.e. $\tau_i = r_i$.

Hence, differentiating (40) w.r.t time yields the dynamics of set-point generator given by

$$\dot{x}_i = \begin{bmatrix} \dot{p}_i^d - \dot{\tau}_i \\ \dot{q}_i^d \end{bmatrix} = \begin{bmatrix} -\sum_{j\in N_i} e_{ij}^p + S(\tau_i)e_{ij}^o - S(\omega_i)\tau_i \\ -\sum_{j\in N_i} \frac{1}{2}U(q_i^d)e_{ij}^o \end{bmatrix}$$
$$= \begin{bmatrix} -\sum_{j\in N_i} e_{ij}^p \\ -\sum_{j\in N_i} \frac{1}{2}U(q_i^d)e_{ij}^o \end{bmatrix}, \tag{42}$$

where the rotational error $-\sum_{j\in N_i} S(\tau_i)e_{ij}^o$ and the time-derivative of the displacement vector $-S(\omega_i)\tau_i$ cancel out as $\omega_i = \sum_{j\in N_i} e_{ij}^o$ and $S(\omega_i)\tau_i = -S(\tau_i)\omega_i$. Hence, the transformation results in a decoupling of the translational motion from the rotational one. Since $e_{ij}^p = (p_i^d - \tau_i) - (p_j^d - \tau_j)$ and $e_{ij}^o = U(q_i^d)^\intercal(q_i^d - q_j^d)$ the dynamics (42) constitute a consensus protocol for the translational and rotational set-points. With the transformation (40) the constraints (23) and (24) for the desired set-points p^d and q^d are given by

$$x_i = x_j, \tag{43}$$

which defines the transformed kinematic constraints.

G. Human operator to guide multiple robots as leader

For the sake of readability we reformulate the proposed formation-based set-point generator interfaced by a human operator in a more compact fashion so that the later performed stability and controllability analysis is done more conveniently. The reformulation is done without any modification or adaptation to the approach. Partially following the argumentation in [29], we can compactly rewrite (42) using (4b) and (37). By doing so the human-extended dynamical system which involves the input of the human is given by

$$\dot{\bar{x}} = -\begin{bmatrix} \bar{L}\otimes I_3 & 0 \\ 0 & \frac{1}{2}\bar{\mathscr{U}}(x^q, q_h)(\bar{L}\otimes I_4) \end{bmatrix}\bar{x} \tag{44}$$

where $\bar{L}$ is the human-extended Laplacian matrix which can be decomposed as

$$\bar{L} = -\left[\begin{array}{c|c} A_{\text{fms}} & b_{\text{fms}} \\ \hline b_{\text{fms}}^\intercal & \gamma \end{array}\right], \tag{45}$$

and $\bar{x} = \left[x^{p\intercal}, x_h^\intercal, x^{q\intercal}, q_h^\intercal\right]^\intercal \in \mathbb{R}^{7(N+1)}$ is the concatenated pose and $x^p = \left[x_1^{p\intercal}, \ldots, x_N^{p\intercal}\right]^\intercal \in \mathbb{R}^{3N}$ and $x^q = \left[x_1^{q\intercal}, \ldots, x_N^{q\intercal}\right]^\intercal \in \mathbb{R}^{4N}$ is the concatenated position and quaternion vector. The matrix $\bar{L} \in \mathbb{R}^{N\times N}$ is the graph Laplacian. Furthermore, the matrix $\bar{\mathscr{U}}(x^q, q_h) \in \mathbb{R}^{4N\times 4N}$ is defined as $\bar{\mathscr{U}}(x^q, q_h) = \text{diag}(I_4 - x_1^q x_1^{q\intercal}, \ldots, I_4 - q_h q_h^\intercal)$.

Here, A_{fms} is the principal submatrix of $\bar{L}$ and reflects the influence of the cooperating robots on each other. Accordingly, $b_{\text{fms}} \in \mathbb{R}^N$ represents the influence of the human leader on the team of robots. Similar to [8], $A_{\text{fms}} \in \mathbb{R}^{N\times N}$ and $b_{\text{fms}} \in \mathbb{R}^N$ are the system and input matrices of the controlled consensus problem resulting from the graph Laplacian. It is generally known that 0 is an eigenvalue of L belonging to the eigenvector 1 [30]. Due to the decomposition (45) a relationship between A_{fms} and b_{fms} is then given by

$$A_{\text{fms}}1 = -b_{\text{fms}}. \tag{46}$$

Here, $-L$ is known to be symmetric and negative semi-definite. Due to Cauchy's interlacing theorem, A_{fms} is then negative definite, i.e. all eigenvalues are negative [31]. Both A_{fms} and b_{fms} result from the neighborhood topology of the formation control law. More precisely, b_{fms} contains entries with 1 and 0, where a 1-entry at the kth position indicates that the kth robot is a neighbor of the human. So b_{fms} is the direct representation of N_h as a vector as the k-entry of b_{fms} is 1 if $k \in N_h$. Hence, the desired position x_k of the kth robot is directly influenced by u_h. We assume the following for b_{fms}.

Assumption 4: The vector $b_{\text{fms}} \neq 0$ i.e. at least one robotic manipulators has access to the human's input u_h.

Yet as there is no direct physical contact between the human and the robot team, the human only imposes movements on the robot-formation by his/her arm movement. From a control theoretic perspective the human has only a directed influence on the states of the robot team. The opposite direction is not true as the team of cooperating robots has no direct influence on the human operator. Due to that the dynamics of the human motion (44) represented by $\dot{x}_h = (b_{\text{fms}}^\intercal \otimes I_3)x^p + (\gamma \otimes I_3)x_h$ and $\dot{q}_h = \frac{1}{2}\mathscr{U}(q_h)(b_{\text{fms}}^\intercal \otimes I_4)q^d + \frac{1}{2}\mathscr{U}(q_h)(\gamma \otimes I_4)q_h$ must be neglected. We obtain the leader-follower dynamics describing the human-to-robots interaction. The dynamical system representing the human influence on the set-points is given by

$$\dot{x}^p = (A_{\text{fms}} \otimes I_3)x^p + (b_{\text{fms}} \otimes I_3)x_h \tag{47a}$$
$$\dot{x}^q = \frac{1}{2}\mathscr{U}(x^q)((A_{\text{fms}} \otimes I_4)x^q + (b_{\text{fms}} \otimes I_4)q_h), \tag{47b}$$

where $\mathscr{U}(x^q)$ is defined similar to $\bar{\mathscr{U}}(x^q, q_h)$ and can be simplified using (4a) as $\mathscr{U}(x^q) = \text{diag}(I_4 - x_1^q x_1^{q\intercal}, \ldots, I_4 - x_N^q x_N^{q\intercal})$.

Remark 4: Some readers might now wonder what the advantage of using the dynamics (47) for generating the set-points $p_i^d = x^p + d_{ih}$ and $q_i^d = x_i^q$ over using the differential kinematics $v_i^d = G_i(d_{ih})^\intercal v_h$ described by the grasp matrix in (11) is, where v_h is the time-derivative of u_h. Note here that d_{ih} represents the *measured* grasp geometry. Any error in d_{ih} accumulates over time in p_i^d as the time-integral of $v_i^d = G_i(d_{ih})^\intercal v_h$. Hence, internal forces (32) increase unboundedly. In the presented formation-based approach the grasp geometry is decomposed from the dynamics as a constant offset in (40) yielding a constant internal force.

For illustration we present an example now.

Example 3: Assume now three equal robots defined in Example 1 and 2. For this example we have $N_1 = \{2,3,h\}$, $N_2 = \{1,3\}$, $N_3 = \{1,2,h\}$, and $N_h = \{1,3\}$. The set-points x_1, x_2, x_3 are generated by (47) which yields

$$\dot{x} = \begin{pmatrix} -3 & 1 & 1 \\ 1 & -2 & 1 \\ 1 & 1 & -3 \end{pmatrix}\begin{pmatrix} x_1 \\ x_2 \\ x_3 \end{pmatrix} + \begin{pmatrix} 1 \\ 0 \\ 1 \end{pmatrix} x_h. \tag{48}$$

At this point we are ready to convey the main message of this section depicted in Fig. 4 by linking the concepts and equations introduced throughout this section with the high conceptual level from the beginning. By moving his/her arm the human operator produces an input u_h which corresponds e.g. to the pose of his/her palm. The human input u_h is measured externally and communicated to the robots. Based on u_h the

set-points ξ^d are computed by (47) in accordance with the set points of the other robots. The robots share their set-points over network. The particular set-points ξ_i^d of the concatenated vector ξ^d induce a motion ξ_i of the locally impedance-controlled manipulators (1). Since the manipulators rigidly grasp the object, the constraints (9) hold and a motion ξ_o is also induced on the object (7). By using Gauss' principle of least constraint the object motion ξ_o, which is induced by the set-points ξ_i^d, is characterized by the dynamics (22).

III. Stability

In this work we investigate the Lyapunov stability of the overall system from a *constant* human input u_h to the output of the multi-robot cooperative manipulation task ξ_o. The equilibria of (47) and (22) are discussed separately since the equilibria of the human-guided set-point generator (47) and their stability are independent of (22). By doing so we can directly observe if the equilibria are in line with the constraints in a cooperative manipulation task. The equilibria of the impedance-based multi-robot dynamics (22) and their stability are then discussed both generally for any set-points and then in particular for the set-points equilibria generated by the human input in (47). Consequently, the separate equilibria discussion does not only produces a more intelligible result but also provides us with more insights.

A. Equilibria and stability of the set-point generation

Given a specific human input u_h we are at first interested what the resultant desired set-points ξ^d are. In other words we are ready to derive the equilibiria of the set-point generator (47) and their stability properties. The stability of the set-point generator (47) for a constant human input u_h is analyzed in this section. Please note here at this stage that due to the use of quaternions $q_i^d = q_h$ and $q_i^d = -q_h$ stands for the same physical rotation. Hence, there are exist two possible equilibria for the set-point generator which is formally stated in Proposition 1. In Proposition 2 we subsequently show that $q_i^d = q_h$ is the only stable equilibrium.

Proposition 1: Under Assumptions 3 and 4 the human-guided set-point generator (47) has the following two equilibria for all robotic manipulator i

$$\xi_i^d = \begin{pmatrix} p_i^d \\ q_i^d \end{pmatrix} = \begin{pmatrix} x_h + d_{ih} \\ q_h \end{pmatrix} \quad \text{and} \tag{49}$$

$$\xi_i^d = \begin{pmatrix} p_i^d \\ q_i^d \end{pmatrix} = \begin{pmatrix} x_h + d_{ih} \\ -q_h \end{pmatrix}. \tag{50}$$

Proof: The equilibria of (47) are determined by $\dot{x}^p = 0$ and $\dot{x}^q = 0$. We start with the set-point generator for the desired robot orientations (47b) here as

$$0 = \frac{1}{2}\mathscr{U}(x^q)\left((A_{\text{fms}} \otimes I_4)x^q + (b_{\text{fms}} \otimes I_4)q_h\right), \tag{51}$$

where we substitute (46) for b_{fms} and employ $(A_{\text{fms}} 1 \otimes I_4) = (A_{\text{fms}} \otimes I_4)(1 \otimes 1)$ to rewrite (51) as

$$0 = \frac{1}{2}\mathscr{U}(x^q)(A_{\text{fms}} \otimes I_4)\left(x^q - (1 \otimes q_h)\right). \tag{52}$$

It is obvious that the trivial solution $q^d = (1 \otimes q_h)$ satisfies (52). Note here that $(A_{\text{fms}} \otimes I_4)$ is full-rank and the A_{fms} matrix has only integer entries. Hence, a solution of (52) can also lie in the null-space of the matrix $\mathscr{U}(x^q)$ which is given by (4b). Due to that and the fact that the null-space must be an integer combination of x_i^q and q_h the solution of (52) is $x_i^q = \pm q_h$. Consequently, we obtain the equilibria of the translational set-point generator (47a) by setting $\dot{x}^p = 0$ as $0 = (A_{\text{fms}} \otimes I_3)x^p + (b_{\text{fms}} \otimes I_3)x_h$ and the equilibria of (47a) are

$$x^p = (-A_{\text{fms}}^{-1} b_{\text{fms}} \otimes I_3)x_h = 1 \otimes x_h, \tag{53}$$

where we use (40) and (41) to see that

$$p_i^d = x_h + d_{ih}, \tag{54}$$

which concludes our proof. ∎

We now define a set of manipulator set-points which only excludes the equilibrium (50) given by

$$\Omega_{\text{fms}} = \{\xi_i^d = \begin{pmatrix} p_i^d \\ q_i^d \end{pmatrix} | p_i^d \in \mathbb{R}^3, q_i^d \in SO(3) \cap q_i^d \neq -q_h\}$$

We are now ready to state the stability of the set-point generator.

Proposition 2: Let Assumptions 3 and 4 hold and let the initial states $\xi_i^d(t_o) \in \Omega_{\text{fms}}$. Then the equilibrium (49) of the set-point generator (47) is asymptotically stable.

Proof: To show stability of set-point generator (47) we employ the following Lyapunov function candidate

$$V_{\text{fms}} = \frac{1}{2}\bar{x}^\intercal(\bar{L} \otimes I_7)\bar{x} \tag{55}$$

where the human-extended Laplacian matrix $\bar{L}$ is defined in (45). Note here that V_{fms} is positive definite and radially unbounded with respect to $x_i - x_j$ and $x_i - u_h$ for all $i \in N$ and $j \in N_i$. Using the fact that $\dot{u}_h = 0$ the time-derivative of V is given by

$$\begin{aligned} \dot{V}_{\text{fms}} &= \bar{x}^\intercal(\bar{L} \otimes I_7)\dot{\bar{x}} \\ &= \left[x^{p\intercal}, x_h^\intercal\right](\bar{L} \otimes I_3)\begin{bmatrix} \dot{\bar{x}}^p \\ 0 \end{bmatrix} + \left[x^{q\intercal}, q_h^\intercal\right](\bar{L} \otimes I_4)\begin{bmatrix} \dot{\bar{x}}^q \\ 0 \end{bmatrix} \\ &= -\dot{x}^{p\intercal}\dot{x}^p - \dot{x}^{q\intercal}\dot{x}^q \leq 0, \end{aligned} \tag{56}$$

where we employ (45) for the human-extended Laplacian $\bar{L}$. Referring to Proposition 1 the set-point generator has two possible equilibria given by (49) and (50). Using (55) it is shown that the equilibrium (49) represents the minimum energy and any perturbation from (49) drives the system to (49). The proof is concluded by stating that $\xi_i^d(t)$ is bounded and the equilibrium (49) is the only point in Ω_{fms} where $\dot{V}_{\text{fms}} = 0$. Hence, due to LaSalles invariance principle Ω_{fms} is the region of attraction in which the equilibrium (49) is asymptotically stable. Hence, (50) is unstable. ∎

B. Equilibria and stability of the interaction dynamics

Given distributed manipulator set-points ξ^d we are now interested in the resultant object pose ξ_o which are the equilibria of the interaction dynamics (22) and their stability properties. The stability of the impedance-based interaction dynamics (22) is analyzed by first deriving the equilibria. We conclude this section by showing asymptotic stability of the interaction dynamics (22) under the proposed set-point generator (47) . Yet before stating the equilibria of (22) we outline the potential solutions of a quaternion error given by

$$U(q_i)^\intercal q_j = e_{ij}^o, \tag{57}$$

where q_i and e_{ij}^o are known and q_j is unknown. The solution $q_j = q_j^*$ is given by

$$q_j^* = \bar{q}_j + \alpha q_i, \tag{58}$$

where $\bar{q}_j$ is any solution of the underdetermined system of linear equations (57). In general there are infinitely many solutions. Yet the solution q_j^* must be a unit quaternion. Then, the scalar weight α is given by

$$\alpha = -q_i^\mathsf{T}\bar{q}_j \pm \sqrt{q_i^\mathsf{T}\bar{q}_j q_i^\mathsf{T}\bar{q}_j + (1-\bar{q}_j^\mathsf{T}\bar{q}_j)}. \tag{59}$$

Hence, the solution set of (57) denoted by q_j^* consists of two unit quaternions.

Proposition 3: Let Assumptions 1 and 2 hold. Then the impedance-based multi-robot dynamics (22) have the equilibria

$$\left(\ v_o^\mathsf{T}, p_o^\mathsf{T}, q_o^\mathsf{T}\ \right)^\mathsf{T} = \left(\ 0, \tfrac{1}{N}\textstyle\sum_i p_i^{d\mathsf{T}} + \tfrac{1}{Nk}\tilde{f}_o^\mathsf{T}, q_o^{*\mathsf{T}}\ \right)^\mathsf{T}, \tag{60}$$

where $q_o = q_o^*$ is a unit quaternion which solves

$$U(\sum_i q_i^d)^\mathsf{T} q_o = \frac{1}{\kappa_i}\tilde{\tau}_o + \frac{k_i}{\kappa_i}\sum_i S(r_i)p_i^d. \tag{61}$$

Proof: The potential equilibria of (22) obviously satisfy $v_o = 0$ and $\dot{v}_o = 0$ which yields

$$\mathscr{K}_o \xi_o = \sum_i \mathscr{K}_i \xi_i^d + \tilde{h}_o, \tag{62}$$

and implies the equilibria of the positions and orientations as

$$\sum_i k_i p_o = \sum_i k_i p_i^d + \tilde{f}_o \tag{63a}$$

$$0 = \sum_i k_i S(r_i)\, p_i^d + \sum_i \kappa_i U(q_o)^\mathsf{T} q_i^d + \tilde{\tau}_o \tag{63b}$$

Solving (63) for p_o, q_o and employing Assumptions 1 and 2 yields (60). Due to (58) there are two rotational equilibria. ■

Proposition 4: Let Assumptions 1 and 2 hold and assume that there is no force disturbance $\tilde{f}_o = 0$. Then the equilibria of the interaction dynamics (22) driven by the distributed set-point generator (47) are

$$\left(\ v_o^\mathsf{T}, p_o^\mathsf{T}, q_o^\mathsf{T}\ \right)^\mathsf{T} = \left(\ 0, x_h^\mathsf{T} + \tfrac{1}{N}\textstyle\sum_i d_{ih}^\mathsf{T}, q_h^\mathsf{T}\ \right)^\mathsf{T} \quad \text{and} \tag{64}$$

$$\left(\ v_o^\mathsf{T}, p_o^\mathsf{T}, q_o^\mathsf{T}\ \right)^\mathsf{T} = \left(\ 0^\mathsf{T}, x_h^\mathsf{T} + \tfrac{1}{N}\textstyle\sum_i d_{ih}^\mathsf{T}, -q_h^\mathsf{T}\ \right)^\mathsf{T}. \tag{65}$$

Proof: The proof is the straightforward application of Propositions 1 and 3. We set $\tilde{f}_o = 0$ and replace the particular set-points p_i^d in (60) by (49). Note here that $\sum_i k_i S(r_i)^\mathsf{T}(x_h + d_{ih}) = 0$ due to Assumption 1 and $d_{ih} = r_i - r_h$. ■

We now define a set of object poses which only excludes the equilibrium (65) given by

$$\Omega_{\text{imp}} = \{\left(\ v_o^\mathsf{T}, p_o^\mathsf{T}, q_o^\mathsf{T}\ \right)^\mathsf{T} | v_o \in \mathbb{R}^6, p_o \in \mathbb{R}^3, q_o \in SO(3) \cap q_o \neq -q_h\} \tag{66}$$

Proposition 5: Let Assumptions 1 and 2 hold. Further, let $\tilde{f}_o = 0$ and the initial state $\left(v_o^\mathsf{T}, p_o^\mathsf{T}, q_o^\mathsf{T}\right)^\mathsf{T} \in \Omega_{\text{imp}}$. Then the equilibrium (64) is asymptotically stable. .

Proof: To show stability of the interaction dynamics (22) we employ the following Lyapunov function candidate

$$V_{\text{imp}} = \frac{1}{2}v_o^\mathsf{T}\mathscr{M}v_o + (\xi_o - \xi_o^d)^\mathsf{T}\begin{bmatrix} \frac{1}{2}kI_3 & 0 \\ 0 & 2\kappa I_4 \end{bmatrix}(\xi_o - \xi_o^d),$$

which is positive definite and radially unbounded with respect to v_o and $(\xi_o - \xi_o^d)$. Due to the usage of the set-point generator (47) the desired object pose ξ_o^d is given by

$$\xi_o^d = \begin{pmatrix} x_h + \frac{1}{N}\sum_i d_{ih} \\ q_h \end{pmatrix} \tag{67}$$

Using (2), (22), (5) the time-derivative of V_{imp} is given by

$$\begin{aligned}\dot{V}_{\text{imp}} &= \frac{1}{2}v_o^\mathsf{T}\dot{\mathscr{M}}v_o + v_o^\mathsf{T}\mathscr{M}\dot{v}_o + \dot{\xi}_o^\mathsf{T}\begin{bmatrix} kI_3 & 0 \\ 0 & \kappa I_4 \end{bmatrix}(\xi_o - \xi_o^d) \\ &= \frac{1}{2}v_o^\mathsf{T}(\dot{\mathscr{M}} - 2\mathscr{C}_o)v_o - v_o^\mathsf{T}\mathscr{D}v_o \\ &\quad + v_o^\mathsf{T}\left(\begin{bmatrix} kI_3 & 0 \\ 0 & 2\kappa U(q_o)^\mathsf{T} \end{bmatrix}\xi_o - h_o^\kappa(\xi_o, \xi_o^d).\right) \\ &= -v_o^\mathsf{T}\mathscr{D}v_o \leq 0,\end{aligned} \tag{68}$$

where a straightforward calculation shows that $\frac{1}{2}v_o^\mathsf{T}(\dot{\mathscr{M}} - 2\mathscr{C}_o)v_o = 0$ which is a consequence of the Hamilton principle of conservation of energy. Note here that $\dot{V}_{\text{imp}}$ is negative semi-definite. We observe that the function candidate V_{imp} decreases as long as $v_o \neq 0$. To find the equilibrium of (22), we have $\dot{V}_{\text{imp}} = 0$ and $v_o = 0$ which rigorously shows that $\dot{V}_{\text{imp}} = 0$ only for (64) and (65). Since $\left(v_o^\mathsf{T}(t), p_o^\mathsf{T}(t), q_o^\mathsf{T}(t)\right)^\mathsf{T}$ is bounded and the equilibrium (64) is the only point in Ω_{imp} where $\dot{V}_{\text{imp}} = 0$, (64) is asymptotically stable due to LaSalle's invariance principle. By investigating the minimum energy of V_{imp} it is shown that Ω_{imp} is the region of attraction for (64). Hence, any perturbation drives the system to (64). ■

Remark 5: We are ready to pinpoint another advantage of using the dynamics (38) and (39) for generating the set-points ξ^d over employing the kinematic relation between the ith end-effector and the object defined in (11). Here, particular manipulator set-points can react to each other which allows the allocation of autonomous capabilities to robots. The presented approach can be easily extended with a collective collision avoidance mechanism for obstacles where the robots are forced to break the formation for safety reasons. When a critical situation is detected the robots switch to a different interaction topology and a collision avoidance scheme (cf. obstacle avoidance with artificial potential field as proposed in [32]). Hence, they initiate a break of the robot formation by opening the rigid grasp. As soon as the critical situation is passed the robots re-establish the formation with the original interaction topology and rigidly re-grasp the object. The stability of this switching system can be analysed with techniques of hybrid control theory, which, however, is beyond the scope of the work here. After establishing the steady-state stability properties of the set-point generator (47) and the multi-robot dynamics (22) we are now ready to investigate the transient behavior of the proposed interaction mechanism.

IV. Guidance by Human Leader

The cooperative robots manipulate an object under a formation-preserving control law while a desired trajectory for the aggregated team of robots is given to the robots by the human operator. Hence, when a human operator issues commands to multiple cooperative robots through the set-point generator (47), the question arises whether the human state u_h

excites all robots simultaneously satisfying the constraint (43) or if particular robots are excited independently from each other violating the constraint (43).

A. Internal force during transient phase

We now have a closer look at if and in which way the distributed set-point generator (47) can induce an internal force. There is no internal force induced if the set-points lie inside the subspace given by (43). If the constraint (43) holds for all manipulator pairs then all x_i are equal. Hence, the concatenated state x can be compactly written using the set-builder notation as

$$\{x \in \mathbb{R}^{7N} | x = [x_1{}^\intercal, \ldots, x_N{}^\intercal]^\intercal \wedge \forall (i,j) : x_i = x_j\} = \{x \in \mathbb{R}^{7N} | x = 1 \otimes \alpha\}, \quad (69)$$

where $1 \in \mathbb{R}^N$ denotes that the movement of the robots must be equal along a particular dimension. Furthermore, $\alpha \in \mathbb{R}^7$ is the free parameters due to a separate scaling of the robots in the particular dimensions. Hence, the subspace which does not induce internal forces by the desired set-points x and their time-derivatives $\dot{x}$ is given by

$$x = 1 \otimes \alpha, \quad \dot{x} = 1 \otimes \dot{\alpha}, \quad (70)$$

where the vector $\dot{\alpha}$ is the time-derivative of α. We can now substitute (70) into (47) and reorder the system as follows

$$\Theta \begin{bmatrix} 1 \otimes I_7 & -A_{\text{fms}} 1 \otimes I_7 \end{bmatrix} \begin{bmatrix} \dot{\alpha} \\ \alpha \end{bmatrix} = \Theta [b_{\text{fms}} \otimes I_7] u_h, \quad (71)$$

where the matrix $\Theta \in \mathbb{R}^{6N \times 7N}$ is defined as $\Theta = \text{diag}(I_3, \ldots, I_3, U(x_1^q)^\intercal, \ldots, U(x_N^q)^\intercal)$. Here we result in a system of linear equations with unknowns $\dot{\alpha}$ and α. The question remains open here whether we can find a solution that satisfies the system (71) w.r.t. the parameters $\dot{\alpha}$ and α. Note here that the solution depends on the matrices A_{fms} and b_{fms}. The solution is independent from Θ as it appears on both sides (71). There exists at least one solution since $-A_{\text{fms}} 1 \otimes I_7$ constitutes the same subspace as $b_{\text{fms}} \otimes I_7$ given in (46). We compare the columns $1 \otimes I_7$ and $-A_{\text{fms}} 1 \otimes I_7$ in comparison with $[b_{\text{fms}} \otimes I_7] u_h$ in order to identify two different cases for the solution of (71) by inspection: (a) For $b_{\text{fms}} \neq 1$ the subspace formed by the first columns $1 \otimes I_7$ is independent from the subspace $b_{\text{fms}} \otimes I_7$. Hence, by inspection we identify the solution of (71) to be $\dot{\alpha} = 0$ and $\alpha = u_h$. The interpretation of this result is as follows: For $b_{\text{fms}} \neq 1$ the operator does not induce an internal force for the static case $\alpha^* = u_h$ and $\dot{\alpha}^* = 0$. Here, the desired set-points are in steady-state. However, as soon as the system states converge, i.e. $\dot{\alpha}^* \neq 0$, an internal force is induced. The states of a dynamical system converging to a steady state is called transient phase. Here, we result in a break-up of the formation during the transient phase of the dynamical system (47). Hence, in the transient phase the desired positions are not geometrically consistent with the object geometry any more. (b) For $b_{\text{fms}} = 1$ each column of $\begin{bmatrix} 1 \otimes I_7 & b_{\text{fms}} \otimes I_7 \end{bmatrix}$ can be represented by $b_{\text{fms}} \otimes I_7$. Hence, there exist infinitely many solutions for $\dot{\alpha}$ and α such that the human operator does not induce an internal force. We are now ready to state the final result relating the internal force and N_h.

Proposition 6: Let $h \in N_i, \ \forall i \in \{1, \ldots N\}$ in (38) and (39). Then no internal force (32) is induced through the set-point generator (47) by u_h.

Proof: If $h \in N_i, \ \forall i \in \{1, \ldots N\}$ in (38) and (39), then the human input u_h is made accessible to all robots. If the human state can be accessed by all robots, we have $b_{\text{fms}} = 1$. As discussed before for $b_{\text{fms}} = 1$ the constraint for cooperative manipulation (43) is satisfied in both steady-state and transient phase. If there is no divergence of the desired trajectories, i.e. (43) is satisfied, then there is no internal force acting on the object (32) which is caused by the input u_h. ■

The subspace, which is independently influenced by the human operator, is closely related to the controllability of a system. As previously commented for (71) the controllability question is the same for both translational and rotational movements. Due to that we restrict ourselves to the analysis of the matrix pair A_{fms} and b_{fms} in the following.

Remark 6: At first sight the consequence of Proposition 6 is unexpected from a formation-based perspective as it is only relevant that the human state information can be accessed by by all robots i.e. $h \in N_i, \ \forall i \in \{1, \ldots N\}$ in (38) and (39). No information exchange between the robots is relevant in order to permanently satisfy the constraints in the cooperative manipulation task. From cooperative manipulation perspective the result is not surprising. Usually a virtual frame ξ_o is attached to the object. The grasp matrix G defined in (13) describes the kinematics. G generates desired end-effector velocities $\dot{v}$ based on the desired object velocity $\dot{v}_o$ given by $\dot{v} = G^\intercal \dot{v}_o$. Here, $G^\intercal$ is a mapping from ξ_o to *all* ξ_i. If we now interpret ξ_o as the leader then the grasp matrix defines a special case of the proposed set-point generator where the leader directly commands all followers and the system matrices are given by $A_{\text{fms}} = -I_N$ and $b_{\text{fms}} = 1$.

B. Human shared control

The influence of the human input on particular set-points plays a major role here and from a system theoretical perspective the influence of inputs on system states is defined as a controllability. Although our leader-follower system (47) is defined for six dimensions in space, we investigate here only the controllability of one dimension. As discussed earlier for (71) the controllable subspace of the set-point generator (47) only depends on the matrix pair $(A_{\text{fms}}, b_{\text{fms}})$ and not on the matrix Θ. As the matrix Θ only maps the input onto the subspace of quaternions and is always rank $3N$ we can neglect this matrix in the following analysis. Hence, our system dynamics of (47) simplifies as

$$\dot{x} = A_{\text{fms}} x + b_{\text{fms}} u, \quad (72)$$

where x is one state of x^p or x^q along one direction in space and u is the human input in that direction. Without loosing any insight this argumentation simplifies our analysis.

In the controllability discussion we employ methods such as Kalman decomposition and eigenvalue analysis to interpret our results. The controllability matrix Q_{fms} of the matrix pair $(A_{\text{fms}}, b_{\text{fms}})$ is defined as:

$$Q_{\text{fms}} = \begin{bmatrix} b_{\text{fms}} & A_{\text{fms}} b_{\text{fms}} & \ldots & A_{\text{fms}}^{N-1} b_{\text{fms}} \end{bmatrix}. \quad (73)$$

Here we focus on the analysis of the rank of Q_{fms} which characterizes the number of independently controllable states of x^p or x^q along one direction in space. If Q_{fms} is rank

deficient the cooperating multi-robot system (72) can be decomposed into its controllable and uncontrollable part by the Kalman decomposition- The similarity transformation of the Kalman decomposition is given by $T = \left[Q_{\text{fms}}^{\parallel} \mid Q_{\text{fms}}^{\perp} \right]$, where $Q_{\text{fms}}^{\parallel} = \text{span}(Q_{\text{fms}}) \in \mathbb{R}^{N \times \text{rank}\, Q_{\text{fms}}}$ indicates the range of the controllable subspace and $Q_{\text{fms}}^{\perp} = \text{null}(Q_{\text{fms}})$ the range of the uncontrollable subspace. Due to this eigencomposition the similarity transformation results in

$$T^{\intercal} A_{\text{fms}} T = \begin{bmatrix} A_{\text{fms}}^{c} & 0 \\ 0 & A_{\text{fms}}^{\bar{c}} \end{bmatrix}, \quad T^{\intercal} b_{\text{fms}} = \begin{bmatrix} b_{\text{fms}}^{c} \\ 0 \end{bmatrix}, \quad \text{and} \quad \begin{bmatrix} \tilde{x}^{c} \\ \tilde{x}^{\bar{c}} \end{bmatrix} = T^{\intercal} \tilde{x}, \tag{74}$$

where c and $\bar{c}$ correspond to the controllable and uncontrollable parts of the robotic system and result in two decoupled subsystems. Due to the similarity transformation T the eigenvalues denoted as spectrum $\{\lambda_i^{A_{\text{fms}}}\}$ of A_{fms} and of $T^{\intercal} A_{\text{fms}} T$ are the same. The spectrum of A_{fms} is $\{\lambda_i^{A_{\text{fms}}}\} = \{\lambda_i^{A_{\text{fms}}^{c}}\} \cup \{\lambda_i^{A_{\text{fms}}^{\bar{c}}}\}$ where $\lambda_i^{A_{\text{fms}}^{c}}$ is the spectra of $A_{\text{fms}}^{c} \in \mathbb{R}^{\text{rank}\, Q_{\text{fms}} \times \text{rank}\, Q_{\text{fms}}}$ and $\lambda_i^{A_{\text{fms}}^{\bar{c}}}$ is the spectra of $A_{\text{fms}}^{\bar{c}} = \in \mathbb{R}^{N - \text{rank}\, Q_{\text{fms}} \times N - \text{rank}\, Q_{\text{fms}}}$.

The derivation of the constraint (43) for x in (72) yields $x \equiv 1$. It is transformed into the space of controllable and uncontrollable states using the similarity transformation (74) as

$$T^{\intercal} 1 = \begin{bmatrix} Q_{\text{fms}}^{\parallel}{}^{\intercal} \\ Q_{\text{fms}}^{\perp}{}^{\intercal} \end{bmatrix} 1 = \begin{bmatrix} v_k \\ 0 \end{bmatrix} \tag{75}$$

where the constraint-satisfying vector for the controllable subspace is given by $v_k = Q_{\text{fms}}^{\parallel}{}^{\intercal} 1 \in \mathbb{R}^{\text{rank}(Q_{\text{fms}})}$. Note that for the uncontrollable subspace $Q_{\text{fms}}^{\perp}{}^{\intercal} 1$ is always 0 due to the relation (46) between A_{fms} and b_{fms} which results in $1 = -A_{\text{fms}}^{-1} b_{\text{fms}}$. The inverse A_{fms}^{-1} can be expressed using the Cayley-Hamilton theorem as

$$A_{\text{fms}}^{-1} = \frac{(-1)^{N-1}}{\det A_{\text{fms}}} (A_{\text{fms}}^{N-1} + c_{N-1} A_{\text{fms}}^{N-2} + \ldots + c_1 I_N), \tag{76}$$

where c_k are the coefficients of the characteristic polynomial. As A_{fms}^{-1} is a linear combination of the matrices $I_3, \ldots A_{\text{fms}}^{N-1}$, $-A_{\text{fms}}^{-1} b$ it forms the same subspace as the controllability matrix Q_{fms} and its span $Q_{\text{fms}}^{\parallel}$ derived in (73). By definition $Q_{\text{fms}}^{\perp}$ is orthogonal $Q_{\text{fms}}^{\parallel}$ and so $-Q_{\text{fms}}^{\perp} A_{\text{fms}}^{-1} b = 0$.

The meaning of the controllable subspace in case of a multi-robot formation remains unanswered until now. i.e. what is the resulting state after applying the transformation $T = \left[Q_{\text{fms}}^{\parallel} \mid Q_{\text{fms}}^{\perp} \right]$. In general, one has to analytically apply this similarity transformation to derive the controllable states x^c based on the robot state x. In the following we interpret the decomposition (74) from a shared control perspective where the uncontrollable subsystem is the autonomous robotic task and the controllable subsystem is the human task.

1) Autonomous robotic task

By means of shared control the uncontrollable subsystem

$$\dot{x}^{\bar{c}} = A_{\text{fms}}^{\bar{c}} x^{\bar{c}} \tag{77}$$

can be interpreted as the autonomous sub-task of the overall robotic system. Uncontrollability means that the human has no influence on states $x^{\bar{c}}$, i.e. the movement of the human hand has no effect on the transformed robot states. Since the human has no influence on the uncontrollable subsystem, the eigenmodes $\{\lambda_i^{A_{\text{fms}}^{\bar{c}}}\} \subset \{\lambda_i^{A_{\text{fms}}}\}$ are masked from the human. The uncontrollable subsystem $\dot{x}^{\bar{c}} = A_{\text{fms}}^{\bar{c}} x^{\bar{c}}$ is known [31] to be asymptotically stable, i.e. $\lim_{t \to \infty} x^{\bar{c}} = 0$. As the system is asymptotically stable and as the initial condition can be freely chosen as $x^{\bar{c}}(t_0) = 0$ we always have

$$x^{\bar{c}} = 0. \tag{78}$$

We conclude that the uncontrollable states $x^{\bar{c}}$ are always zero as defined in (78) and come up with the formal statement.

Proposition 7: There is no internal force (32) induced by the uncontrollable system (77).

Proof: As we can freely choose the initial condition for (47) to be $x^{\bar{c}}(t_0) = 0$ and the uncontrollable subsystem (77) is asymptotically stable, the uncontrollable states are always 0 which is described in (78). Here, $x^{\bar{c}} = 0$ means that the uncontrollable states $x^{\bar{c}}$ lie in the same subspace as the constraint-satisfying vector derived in (75). As the constraint (43) is satisfied, we have $x = 1$. Due to that there is no internal force (32). ■

This result is desired as the human has no influence on the uncontrollable subsystem. However, it remains unanswered wether the controllable subsystem can cause internal forces.

2) Human guiding sub-task

From a shared control perspective, the controllable subsystem

$$\dot{x}^{c} = A_{\text{fms}}^{c} x^{c} + b_{\text{fms}}^{c} u \tag{79}$$

can be interpreted as the sub-task of the human operator to the system. Before discussing the influence of the human on the particular robot states we first introduce a relation between $\text{rank}(Q_{\text{fms}})$ to the human input vector b_{fms}. In particular we consider the case $b_{\text{fms}} = 1$ which follows from Prop. 6.

Proposition 8: The single-leader dynamics (72) has only one controllable eigenmode if and only if $b_{\text{fms}} = \mathbf{1}$.

Proof: The proof of sufficiency assumes that $b_{\text{fms}} = \mathbf{1}$. Since A_{fms} is the principal submatrix of the Laplacian $-L$ (45), the row sum of A_{fms} is -1. Hence, $A_{\text{fms}} b_{\text{fms}} = -\mathbf{1}$. Iteratively, one can show that $A_{\text{fms}}^{k} b_{\text{fms}} = (-1)^k \mathbf{1}$. Consequently, the controllability matrix $Q_{\text{fms}} = \left[\mathbf{1}, -\mathbf{1}, \mathbf{1}, \ldots, (-1)^{N-1} \mathbf{1} \right]$ has $\text{rank}\,(Q_{\text{fms}}) = 1$. For the proof of necessity, to have a single controllable eigenmode, $\text{rank}(Q_{\text{fms}}) = 1$ and so all columns of the controllability matrix Q_{fms} must be linearly dependent. Hence, there must exist an input vector b_{fms} such that $b_{\text{fms}} = \alpha A_{\text{fms}} b_{\text{fms}}$, where $\alpha \in \mathbb{R}$. By construction we always have $-A_{\text{fms}} \mathbf{1} = b_{\text{fms}}$. Since A_{fms} is always regular [31], $\alpha = -1$ and $\mathbf{b}_{\text{fms}} = \mathbf{1}$. For $A_{\text{fms}}^{2} b_{\text{fms}}, \ldots, A_{\text{fms}}^{N-1} b_{\text{fms}}$ this can be shown iteratively. ■

For $b_{\text{fms}} = \mathbf{1}$ we have a single controllable mode which is the only interaction topology that satisfies the constraint (43). Hence, we propose that the human leader controls a single eigenmode. We now illustrate the controllability analysis.

Example 4: We continue with the previously defined dynamics from Ex. 1, 2 and 3. The controllability matrix Q_{fms} (73) of the set-point generator (48) from Ex. 3 reads as

$$Q_{\text{fms}} = \begin{pmatrix} 1 & -2 & 6 \\ 0 & 2 & -8 \\ 1 & -2 & 6 \end{pmatrix}. \tag{80}$$

By inspection we can observe that the first and third row of Q_{fms} are equal and so $\text{rank}(Q_{\text{fms}}) = 2$. We have $\text{rank}(Q_{\text{fms}}) > 1$ as $N_h \neq \{1,2,3\}$ which results in an internal force as derived in Prop. 6. Let now $N_h = \{1,2,3\}$ and $N_2 = \{1,3,h\}$ based on Prop. 6 the set-point generator dynamics are given by

$$\dot{x} = \begin{pmatrix} -3 & 1 & 1 \\ 1 & \mathbf{-3} & 1 \\ 1 & 1 & -3 \end{pmatrix} \begin{pmatrix} x_1 \\ x_2 \\ x_3 \end{pmatrix} + \begin{pmatrix} 1 \\ 1 \\ 1 \end{pmatrix} x_h. \tag{81}$$

Note here that the difference between (48) and (81) is highlighted bold. Using (81) as set-point generator there is no deviation of the set-points x_1, x_2, x_3 during the transient phase and no internal force f_i^{int} given by (32), which is depicted in Fig. 5 for the human input x_h being a unit step at $t = 1s$.

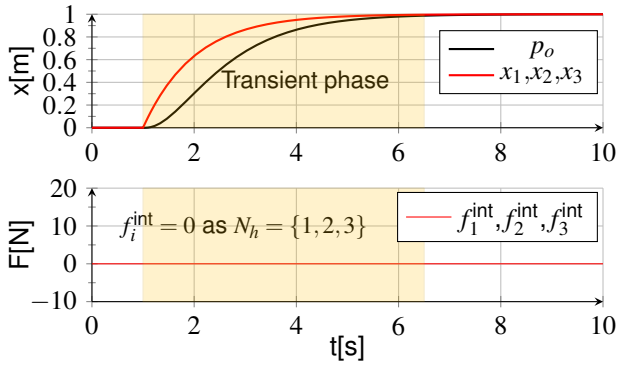

Fig. 5. Object trajectory p_o resulting from distributedly generated robot set-points x_1, x_2, x_3. No deviation of the set-points in the transient between $t = 1s$ and $t = 6.5s$ and so no internal force $f_i^{\text{int}} = 0$.

C. Weighted set-point generators

In this section we present an approach which can significantly decrease internal stress for any interaction topology by the introduction of weights. The idea is to increase the convergence rate of the desired-set points which cause internal forces. Therefore we rewrite our set-point generating dynamics (72) as:

$$\dot{x} = \Gamma A_{\text{fms}} x + \Gamma b_{\text{fms}} u, \tag{82}$$

where $\Gamma = \text{diag}(\gamma_1, \ldots, \gamma_N)$ is a block-diagonal matrix with the entries being $\gamma_i > 0 \in \mathbb{R}$ are scalar weights in order to allocate different speeds to different set-points.

Before introducing a formal result which relates the weights γ_i to the internal force h^{int} we re-label our set-point generator (82). This can be done without loss of generality and is performed here for the sake of exposition. Note here that all properties of the graph Laplacian remain since a re-labeling is just an isormophism of a graph. First we collect the states of all agents i belonging to the set N_h into the state $\tilde{x}_2 \in \mathbb{R}^{1^\intercal b_{\text{fms}}}$ where $1^\intercal b_{\text{fms}}$ denotes the number of all direct neighbors. Analogously we put the states of all the remaining robots which are not in neighborhood N_h of the human into the state $\tilde{x}_1 \in \mathbb{R}^{N-1^\intercal b_{\text{fms}}}$. Furthermore, in our setup the weights are only different with respect to the previously defined two groups, i.e. the state $\tilde{x}_1$ evolves with speed γ_1 and $\tilde{x}_2$ evolves with γ_2. Hence, we have $\Gamma = \text{diag}(\gamma_1 I_{1^\intercal b_{\text{fms}}}, \gamma_2 I_{N-1^\intercal b_{\text{fms}}})$. By using that collocation for notation and by an appropriate decomposition of A_{fms} as

$$A_{\text{fms}} = \begin{bmatrix} A_{f1} & B_{f1} \\ B_{f1}^\intercal & A_{f2} \end{bmatrix}$$

we can rewrite (82) as follows:

$$\begin{bmatrix} \dot{\tilde{x}}_1 \\ \dot{\tilde{x}}_2 \end{bmatrix} = \begin{bmatrix} \gamma_1 A_{f1} & \gamma_1 B_{f1} \\ \gamma_2 B_{f1}^\intercal & \gamma_2 A_{f2} \end{bmatrix} \begin{bmatrix} \tilde{x}_1 \\ \tilde{x}_2 \end{bmatrix} + \begin{bmatrix} 0 \\ \gamma_2 1 \end{bmatrix} u, \tag{83}$$

where the states $\tilde{x}_1$ are not directly influenced by the human input u. Based on this we can formally state a relation between the weights γ_i and the internal force h^{int}.

Theorem 1: Let the weights τ_1 in (83) be $\gamma_1 \to \infty$. Then for any interaction topology the internal force are $h^{\text{int}} \to 0$.

Proof: We show now that for $\gamma_1 \to \infty$ we have that $h^{\text{int}} \to 0$. From (83) we know that we have two interconnected differential equations given by a dynamical system without direct influence of the human

$$\dot{\tilde{x}}_1 = \gamma_1 A_{f1} \tilde{x}_1 + \gamma_1 B_{f1} \tilde{x}_2 \tag{84}$$

and a system with direct influence

$$\dot{\tilde{x}}_2 = \gamma_2 A_{f2} \tilde{x}_2 + \gamma_2 B_{f1}^\intercal \tilde{x}_1 + \gamma_2 1 u. \tag{85}$$

Note here that this is not a decomposition into controllable and uncontrollable subspace as u still has indirect influence on $\tilde{x}_2$ through $\tilde{x}_1$. The equilibrium of (84) where $\dot{\tilde{x}}_1 = 0$ is given by

$$\tilde{x}_1(\infty) = -A_{f1}^{-1} B_{f1} \tilde{x}_2. \tag{86}$$

An error between the state $\tilde{x}_1$ and its equilibrium $\tilde{x}_1(\infty)$ is defined by $e_1 = \tilde{x}_1 - \tilde{x}_1(\infty)$ with which the error dynamics result in $\dot{e}_1 = \gamma_1 A_{f1} e_1$. For the error e_1 we can say that it converges with less or equal to the larger eigenvalue $\lambda_{A_{f1}}^{\max}$ of A_{f1} as

$$e_1(t) = e^{\gamma_1 A_{f1} t} e_1(t_o) \leq e^{\gamma_1 \lambda_{A_{f1}}^{\max} t} e_1(t_o). \tag{87}$$

As $\lambda_{A_{f1}}^{\max} < 0$ and $e_1(t_o)$ is bounded we have

$$\lim_{\gamma_1 \to \infty} e_1(t) = 0, \tag{88}$$

due to which we can always express $\tilde{x}_1$ by its equilibrium involving $\tilde{x}_2$ as $\tilde{x}_1 = -A_{f1}^{-1} B_{f1} \tilde{x}_2$. We later show that e_1 results in a violation of the constraint (43) and results in an internal h^{int}. We continue now by substituting the equilibrium $\tilde{x}_1 = -A_{f1}^{-1} B_{f1} \tilde{x}_2$ into (85) as

$$\dot{\tilde{x}}_2 = \gamma_2 (A_{f2} - B_{f1}^\intercal A_{f1}^{-1} B_{f1}) \tilde{x}_2 + \gamma_2 1 u \tag{89}$$

To investigate the accessible subspace in which $\tilde{x}_2$ moves we now look at controllability matrix (73) and the controllable subspace of (89) defined by

$$Q = \begin{bmatrix} \gamma_2 1 & \gamma_2^2 (A_{f2} - B_{f1}^\intercal A_{f1}^{-1} B_{f1}) 1 \end{bmatrix} = \begin{bmatrix} \gamma_2 1 & \gamma_2^2 (A_{f2} 1 + B_{f1}^\intercal 1) \end{bmatrix} = \begin{bmatrix} \gamma_2 1 & -\gamma_2^2 1) \end{bmatrix}, \tag{90}$$

where we apply the relationships $1 = -A_{f1}^{-1} B_{f1} 1$ and $A_{f2} 1 + B_{f1}^\intercal 1 + 1 = 0$. The relationships result from the decomposition (45) of A_{fms} in L and the fact that $L1 = 0$. Note here that the controllable subspace is 1, i.e. all entries of $\tilde{x}_2$ are equal. By having equal entries in $\tilde{x}_2$ we know that $\tilde{x}_2 \in \tilde{x}_2^* 1$ where $\tilde{x}_2^* \in \mathbb{R}$ is a scaling factor and due to that we know that all entries of $\tilde{x}_2$ are equal. Hence the constraint (43) is satisfied and no internal force occurs here. We are now ready to show that $e_1 \neq 0$ causes an internal force by substituting $\tilde{x}_2 \in \tilde{x}_2^* 1$ and $\tilde{x}_1 = -A_{f1}^{-1} B_{f1} \tilde{x}_2$ into

$$e_1 = \tilde{x}_1 + A_{f1}^{-1} B_{f1} \tilde{x}_2 = \tilde{x}_1 + A_{f1}^{-1} B_{f1} \tilde{x}_2^* 1 = \tilde{x}_1 - \tilde{x}_2^* 1,$$

where we can see that if $\tilde{x}_1 - \tilde{x}_2^* 1 \neq 0$ we have a difference between $\tilde{x}_2$ and $\tilde{x}_1$. Hence, by definition we have a difference between the states of the direct and indirect followers. Due to that difference both $\tilde{x}_1$ and $\tilde{x}_2$ cannot be equal. Hence, the constraint (43) is violated which causes an internal force. However due to (88) we know that there is no internal force $h^{\text{int}} \to 0$ induced by e_1 for $\gamma_1 \to \infty$. ■

For illustration we exemplify the weighted set-point generator.

Example 5: We continue with the previously defined dynamics from Ex. 1, 2 and 3. N_h given in Ex. 3 causes an undesired internal forces and so we introduce weights as $\gamma_1 = 1000$ for the set-points of robot 2 and $\gamma_2 = 1$ for the set-points of robot 1 and 3 in the set-point generator (83), where γ_1 is sufficient large from a practical point of view. Hence, (83) is given by

$$\dot{x} = \begin{pmatrix} -3 & 1 & 1 \\ \mathbf{1000} & \mathbf{-2000} & \mathbf{1000} \\ 1 & 1 & -3 \end{pmatrix} \begin{pmatrix} x_1 \\ x_2 \\ x_3 \end{pmatrix} + \begin{pmatrix} 1 \\ 0 \\ 1 \end{pmatrix} x_h, \quad (91)$$

where difference between (48) and (91) is highlighted bold. The resulting internal force f^{int} in (32) is acceptable for a input x_h being a step function at $t = 1s$ as depicted in Fig. 6.

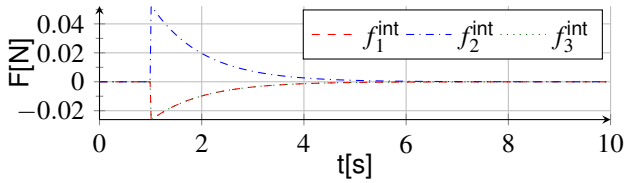

Fig. 6. Internal force $f_i^{\text{int}} \neq 0$ caused by a weighted set-point generator.

In this section we introduced weights for the set-point generator in order to significantly reduce the internal wrench acting on the object based on a controllability analysis. In the next step we discuss controllability of the overall system.

V. Controllability

The influence of the human input on particular set-points gives us fundamental insight in the task. We now extend this result by investigating the controllability of the impedance-based interaction dynamics (22) and the controllability of the overall system in serial connection. Note here that we follow the argumentation in Section IV-B to discuss the controllability of (22) in a single direction of space. Calculating the controllability of (22) with Lie algebra for the translational and rotational motions yields the same result as the simplified version addressing only one direction in space.

A. Controllability of the interaction dynamics

The simplified dynamics of the interaction dynamics (22) in one direction under $\zeta = \left[p_{o,i}, \dot{p}_{o,i}\right]^{\mathsf{T}} \in \mathbb{R}^2$ results as

$$\begin{aligned} \dot{\zeta} &= \begin{bmatrix} 0 & 1 \\ \Pi \sum_{i=1}^{N} k_i & \Pi \sum_{i=1}^{N} d_i \end{bmatrix} \zeta + \begin{bmatrix} 0 \\ \Pi \end{bmatrix} k^{\mathsf{T}} x \\ &= A_{\text{imp}} \zeta + b_{\text{imp}} k^{\mathsf{T}} x, \end{aligned} \quad (92)$$

where $\Pi = -(m_o + \sum_{i=1}^{N} m_i)^{-1}$ and $k = [k_1, \ldots, k_N]^{\mathsf{T}}$. Once again we employ (73) to derive the controllability matrix of the interaction dynamics given by

$$Q_{\text{imp}} = \begin{bmatrix} b_{\text{imp}} & A_{\text{imp}} b_{\text{imp}} \end{bmatrix} = \begin{bmatrix} 0 & \Pi^1 \\ \Pi^1 & \Pi^2 \sum_{i=1}^{N} d_i, \end{bmatrix}, \quad (93)$$

where we can directly observe by inspection that $\text{rank}(Q_{\text{imp}}) = 2$ if $m_o < \infty, m_i < \infty$. So the interaction dynamics of cooperating distributed impedances under a rigid grasp are completely controllable for a single direction in space.

B. Controllability of the overall system

In this section we evaluate the controllability of the simplified versions of the set-point generator (72) and the interaction dynamics (92). The overall state z is then labeled as $z = [x^{\mathsf{T}}, \zeta^{\mathsf{T}}]^{\mathsf{T}}$. To evaluate the controllability of the serial concatenation we have to first setup the complete system dynamics. For a single direction in space the series concatenation of the human-guided set-point generator (72) and the multi-robot interaction dynamics (92) results as

$$A_{\text{tot}} = \begin{bmatrix} A_{\text{fms}} & 0 \\ b_{\text{imp}} k^{\mathsf{T}} & A_{\text{imp}} \end{bmatrix}, \quad b_{\text{tot}} = \begin{bmatrix} b_{\text{fms}} \\ 0 \end{bmatrix} \quad (94)$$

Evaluating the controllability condition (73) of the concatenated system (94) then results in

$$Q_{\text{tot}} = \begin{bmatrix} Q_1^* & \cdots & Q_i^* & \cdots & Q_{N+2}^* \\ Q_1^{**} & \cdots & Q_i^{**} & \cdots & Q_{N+2}^{**} \end{bmatrix}, \quad (95)$$

where the submatrices Q_i^*, Q_i^{**} of Q_{tot} are given as

$$Q_i^* = A_{\text{fms}}^{i-1} b_{\text{fms}} \text{ if } i = 1, \ldots, N+2 \quad \text{and}$$

$$Q_i^{**} = \begin{cases} 0 & \text{if } i = 1 \\ \sum_{j=0}^{i-2} A_{\text{imp}}^{j} b_{\text{imp}} k^{\mathsf{T}} A_{\text{fms}}^{i-2-j} b_{\text{fms}} & \text{if } i = 2, .., N+2 \end{cases}$$

The controllability of serial concatenation of dynamical systems is a rarely studied problem. In general [33] the number of controllable states of the complete system is less or equal to the sum of controllable states of the particular systems:

$$\text{rank}(Q_{\text{tot}}) \leq \text{rank}(Q_{\text{fms}}) + \text{rank}(Q_{\text{imp}}). \quad (96)$$

To avoid internal force acting on the object we stated in Prop. 6 that the human input u is known by all robots, i.e. $b_{\text{fms}} = 1$. Using $A_{\text{fms}}^k b_{\text{fms}} = (-1)^k \mathbf{1}$ and $k^{\mathsf{T}} \mathbf{1} = \sum_{i=1}^{N} k_i$, the overall controllability matrix (95) can then be simplified as

$$Q = \begin{bmatrix} \mathbf{1} & \mathbf{-1} & \mathbf{1} & .. \\ 0 & \sum_{i=1}^{N} k_i b_{\text{imp}} & \sum_{i=1}^{N} k_i (A_{\text{imp}} b_{\text{imp}} - b_{\text{imp}}) & .. \end{bmatrix} \quad (97)$$

As previously derived for b_{fms} we have $\text{rank}(Q_{\text{fms}}) = 1$ and $\text{rank}(Q_{\text{imp}}) = 2$ is always valid. Hence, the rank of the concatenated system results as $\text{rank}(Q) \leq 3$. In our proposed scheme, $b_{\text{fms}} = \mathbf{1}$, we can observe that $\text{rank}(Q_{\text{tot}}) = 3$ by only inspecting the first three columns of (97). From a theoretical perspective the human operator can independently control the set-point of the multi-robot team x, the velocity $\dot{p}_{o,i}$, and the position $p_{o,i}$ of the object in one particular direction in space. We are now ready to experimentally evaluate the proposed interaction mechanism in the next section.

VI. Experiments

The goal of the experimental evaluation is to experimentally validate the previously established theoretical findings of the guidance of a cooperative manipulation task by a single human. We perform large-scale experiments to assess the behaviour of the manipulators in different human-robots formations. We analyze the resulting internal forces, the accuracy, and the sensitivity of the proposed guidance mechanism. In addition, we discuss the technical difficulties which we encountered.

A. Experimental setup

The experimental setup consists of three KUKA LWR 4 manipulating a ball-shaped object which are guided by a human operator, see Fig. 7. The setup is depicted schematically in Fig. 1. Note that this setup has served as basis in the Examples 1- 5 so that the reader had the opportunity to familiarize with the human-guided set-point generator (47) and the impedance-based multi-robot dynamics (22). All relevant control and system parameters are summarized in Table I. A Cartesian impedance control scheme (1) is employed to ensure end-effector compliance while the control loop runs at 1000 Hz. For the sake of exposition we only consider one translational movement denoted by p_i and p_i^d for the manipulators $i = 1,2,3$ in this section without loosing any experimental insights, i.e. we uniformly set $q_i = q_i^d = \text{const}$. Here, $k = 3$ is the most convenient degree of freedom as the desired displacements $d_{ij,3} = 0$ and $d_{ih,3} = 0$ and so $p_i^d = x_i^p,\ \forall i$. During the experiments the human operator wears a marker-equipped handle which determines the input u_h for commanding the robot formation. The Cartesian positions p_1, p_2, p_3 of the three robots and the Cartesian position u_h of the human operator's hand is captured by a passive-marker QualiSys motion capture system at a frequency of 200 Hz. The end-effectors are designed to obtain a quasi-rigid grasp of a ball-shaped object. In our experiments the object is a ball with a diameter of 0.65 m which is maximally inflated to behave like a quasi-rigid object. In order to evaluate different combinations of robotic neighbours, the two scenarios are tested:

(a) Human neighbors as $N_h = \{2,3\}$, $b_{\text{fms}} = [0,1,1]^\intercal$
(b) Human neighbors as $N_h = \{1,2,3\}$, $b_{\text{fms}} = [1,1,1]^\intercal$

The formations (a) and (b) are different with respect to the number of robots directly influenced by the human operator, i.e. by the number of controllable subspaces. The differences between the two formation scenarios are experimentally analyzed with respect to the manipulator motion and the internal force.

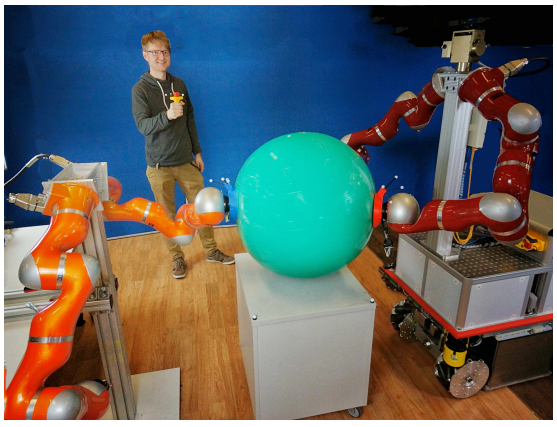

Fig. 7. Human operator controls a group of robots which cooperatively manipulate an object

	Eq.	Values of Parameters
Impedance parameters	(1)	$M = 10I_3$, $D = 120I_3$, $K = 160I_3$
Object parameters	(7)	$m_o = 1.159$
Desired distance between manipulators	(27)	$d_{12} = [0.4,0,0]$ m $d_{23} = d_{13} = [0.2,0.615,0]$ m
Desired distance between manipulators and human	(41)	$d_{1h} = [1.2,0.35,0]$ m $d_{2h} = [0.8,0.35,0]$ m $d_{3h} = [1,0.245,0]$ m
Cooperation weight between manipulators	(82)	$\gamma_i = 2.5, \forall i$

TABLE I
Control parameters used in experiments

B. Technical discussion

This section is a discussion of technical difficulties which we experienced during the experiments. The impedance parameters M_i, D_i, K_i of the individual robots are all selected heuristically since the robotic performance was initially well in the experiments. However, we can state the following observations: all impedance parameters are chosen isotropic and homogenous as discussed in Ass. 1 so that there are no undesired internal forces. To enable an isotropic parametrization of the impedance, the orientation of each robotic manipulator in a common world frame is measured by the Qualisys motion tracking system. In addition, the damping ratio $\zeta_i = \frac{d_i}{2\sqrt{m_i k_i}} = 1.5$ is chosen to be marginally larger than 1, so that the dynamics of the particular manipulators is overdamped and the steady state is reached in adequate time without oscillating.

Until Sec. VI the manipulators are considered to *rigidly* grasp the *rigid* objects while now both the grasp and the object are only quasi-rigid. Both adaptations are necessary in the experiments because each LWR manipulator has only a maximum payload of 7 kg which is relatively low. Note for large objects usually used in cooperative manipulation this payload is drastically reduced to about $1-1.5$ kg due to large torques. The exercise ball is bulky and relatively light.

To compare conditions (a) and (b) the human input trajectory u_h is recorded for reproducibility of the experiment: the human operator moved the worn marker-equipped handle once from an initial to a final configuration, waited for about 1 second and then returned to the initial configuration. The duration of the trajectory $u_h(t)$ is about $10s$ and the covered distance is about $0.5m$. The recorded trajectory $u_h(t)$ is replayed to cope with the conditions (a) and (b) in an equal fashion.

C. Results and discussion for the set-point generator (47)

The dynamics of the human-guided set-point generator (47) are compared with the conditions (a) and (b). The conditions differ in the neighborhood set N_h of the human operator and so different controllable subspaces between (a) and (b) exist: by evaluating (74) for condition (a) we observe that there exist two controllable states $x_1^c = p_1^d$ and $x_2^c = \frac{1}{\sqrt{2}}(p_2^d + p_3^d)$ with different eigenvalues: $\lambda_1^{A_{\text{fms}}^c} = -3.41$ and $\lambda_2^{A_{\text{fms}}^c} = -0.5858$. Since there are two independently controllable subspaces for

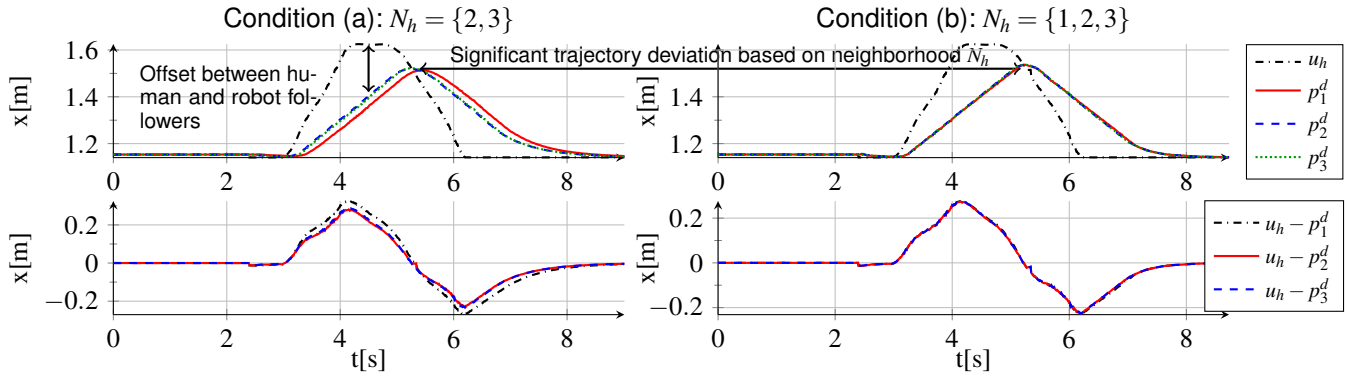

Fig. 8. Three manipulator set-points p_1^d, p_2^d, p_3^d are controlled by the identical human input u_h under different neighborhoods N_h in condition (a) and (b). Different neighborhood topologies result in different controllable subspaces. Hence, the set-point p_i^d in one direction diverge due to different neighborhood $N_h = \{2,3\}$ (top left). For $N_h = \{1,2,3\}$ (top right) there is no deviation between the set-points. During the motion of the object there is a offset between human input u_h and the set-points p_i^d during the transient response of (47). (bottom left for condition (a), bottom right for condition (b))

condition (a) with different eigenvalues of the subspaces, there can be significant deviation of the trajectory p_1^d compared to trajectories p_2^d and p_3^d as shown in Fig. 8. As the human operator has no influence on the uncontrollable subspace $x^{\bar{c}} = \frac{1}{\sqrt{2}}(p_2^d - p_3^d)$, both set-point trajectories p_2^d, p_3^d are equal as depicted on the top left side in Fig. 8.

For condition (b) the locally controllable subspace is the aggregated state $x^c = \frac{1}{\sqrt{3}}(p_1^d + p_2^d + p_3^d)$. Hence, the operator has only access to one controllable subsystem of the multi robot team which moves the desired position p_1^d, p_2^d, p_3^d simultaneously. This is in line with the Prop. 8. Due to that the set-point trajectories p_1, p_2, and p_3 are equal on the top right side in Fig. 8 and there is no breakup of the formation of set-points. By comparing the top left and top right subfigure in Fig. 8 we observe a significant trajectory deviation of p_1^d, p_2^d, and p_3^d based on the neighborhood N_h. Here, we conclude that the theoretical results from Eq. (71) and the subsequent Prop. 6 are validated in the experiments.

During the transient phase there is a offset between between the human input u_h and the manipulator set-points p_i^d for both conditions (a) and (b), i.e. the error term $u_h - p_i^d \neq 0$ for $\dot{u}_h \neq 0$ as depicted in the bottom left and right side in Fig. 8. For both conditions (a) and (b) the maximum positive offset is at approximately $t = 4.1$s and the maximum negative one is at $t = 6.1$s. The offsets can be described with the transient response of the dynamical system representing the human influence on desired set-points (47). Note that the the offset is relative to the settling time and we can tune the settling time with weights as described in (82). For $t > 8s$ the human input u_h is constant again and the offset converges to zero which experimentally demonstrates the stability of the system (47). The stability is theoretically derived in Section III-A.

D. Results and discussion for the multi-robot dynamics (22)

The robotic manipulators grasp the object and the manipulator set-points are driven by (47) under the conditions (a) and (b) using the recorded human input u_h The effect of the different conditions (a) and (b) on the object trajectory p_o is as follows: by comparing the black and dashed line of the left and right side in Fig. 9 we observe no significant effect of the different neighbourhoods N_h on the object trajectory except that the object trajectory excited by the set-point generator in condition (b) converges slightly faster. We assume that this results from the direct influence of the human operator on all three set-points p_i^d simultaneously in condition (b).

Furthermore, we compare for both conditions the measured trajectory from the experiment (black, dashed line) with a simulated trajectory (red, solid line) resulting from the impedance-based multi-robot dynamics (22) which is driven by the same set-point generator (47). The simulated set-point generator is excited by the identical recorded human input u_h. There is a slight deviation between the measured and the simulated trajectory in Fig. 9 which we interpret as a consequence of deviating impedance parameters in theory and experiments. The reason for different impedance parameters can be explained by hardware variations. In total the measured and the simulated trajectory match well which validates the system model for a human-guided cooperative manipulation task, i.e. the series connection modelling of (47) and (22).

Since for condition (a) the deviation of the trajectory of p_1^d is not in compliance with the object geometry an increased measured internal force is acting on the object for this condition, see the black and dashed line on the left side in Fig. 10. For condition (b) with $N_h = \{1,2,3\}$ all manipulator set-points move simultaneously and the internal forces acting on the object are reduced as shown by the black and dashed line on the right side in Fig. 10. This experimental result is formally stated in Section IV-A with the main result as Prop. 6. Again we compare the measured internal force from the experiment (black, dashed line) with a simulated internal force (red, solid line) resulting from the dynamics (47) and (26). For both conditions (a) and (b) the course of measured and simulated internal forces match well. However, a deviation between simulation and measurement is always present which is presumably caused by the force measuring hardware and the deviating impedance parameters as discussed in the previous paragraph. It is experimentally validated that the scenario (b), in which the leader controls only one subspace, results in manipulator motions without considerable deviations and the internal force is significantly reduced.

VII. Conclusions

In this article we propose a control law and a feedback strategy for a robot team controlled by a human in a cooperative manipulation task under a formation-based control approach. By

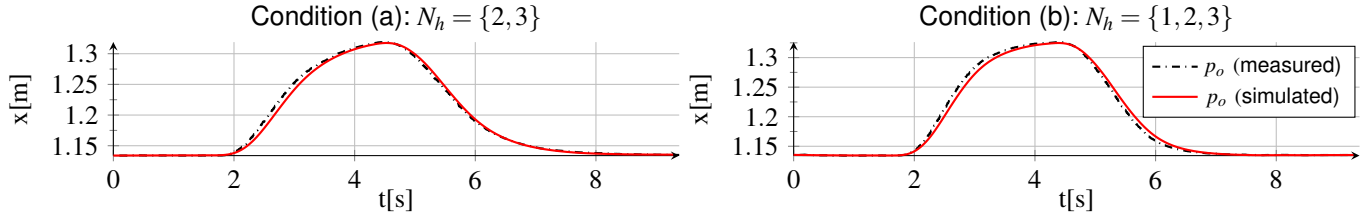

Fig. 9. The object trajectory p_o driven by a human input u_h resulting from different scenario with condition (a) on the left and condition (b) on the right. For each condition the measured trajectory from the experiments is compared with a trajectory from a simulation running the models (47) and (22).

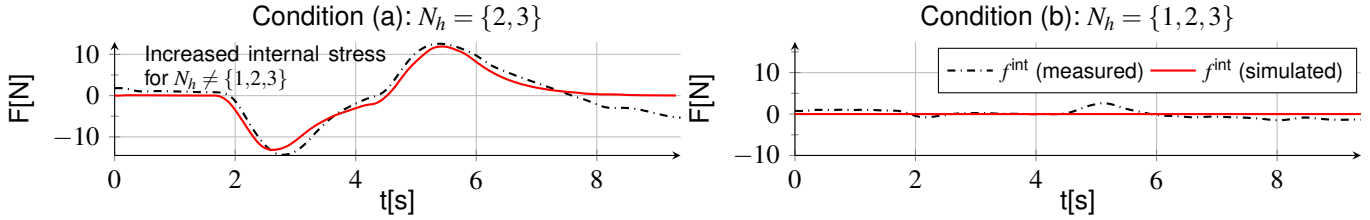

Fig. 10. Internal force acting between manipulator 1 and 3 in direction $k = 3$ resulting from different scenarios with condition (a) on the left and condition (b) on the right. The internal force is significantly increased for condition (a) where $N_h \neq \{1,2,3\}$. For each condition the measured internal force from the experiments is compared with an internal force from a simulation running the model (47) and (26).

analyzing the controllability of such a human-robot formation we deduce that a one-to-all connection is beneficial for the manipulation task in terms of limiting undesired internal forces. The effectiveness and quality of the virtual formation for cooperative manipulation is successfully demonstrated in experiments. For future work, we plan to introduce various autonomous capabilities to cooperative robots and to equip the human operator with wearable devices for task-dependent feedback.

REFERENCES

[1] S. Erhart *et al.*, "An impedance-based control architecture for multi-robot cooperative dual-arm mobile manipulation," in *Proc. IEEE/RSJ IROS*, 2013, pp. 315–322.

[2] D. Sieber *et al.*, "Formation-based approach for multi-robot cooperative manipulation based on optimal control design," in *Proc. IEEE/RSJ IROS*, 2013, pp. 5227–5233.

[3] J. Silvério *et al.*, "Learning bimanual end-effector poses from demonstrations using task-parameterized dynamical systems," in *Proc. IEEE/RSJ IROS*. IEEE, 2015, pp. 464–470.

[4] R. Parasuraman *et al.*, "A model for types and levels of human interaction with automation," *IEEE SMC*, vol. 30, no. 3, pp. 286–297, 2000.

[5] A. Franchi *et al.*, "A passivity-based decentralized approach for the bilateral teleoperation of a group of uavs with switching topology," in *Proc. IEEE ICRA*, 2011, pp. 898–905.

[6] D. Lee and M. W. Spong, "Bilateral teleoperation of multiple cooperative robots over delayed communication networks: theory," in *Proc. IEEE ICRA*, 2005, pp. 360–365.

[7] C. I. Aldana *et al.*, "Leader-follower pose consensus for heterogeneous robot networks with variable time-delays," in *World Congress*, vol. 19, no. 1, 2014, pp. 6674–6679.

[8] J.-P. de la Croix and M. Egerstedt, "Controllability characterizations of leader-based swarm interactions." in *AAAI Fall Symposium: Human Control of Bioinspired Swarms*, 2012.

[9] L. Consolini *et al.*, "Leader–follower formation control of nonholonomic mobile robots with input constraints," *Automatica*, vol. 44, no. 5, pp. 1343–1349, 2008.

[10] S. Scheggi *et al.*, "Human-robot formation control via visual and vibrotactile haptic feedback," *IEEE Transactions on Haptics*, vol. 7, no. 4, pp. 499–511, 2014.

[11] N. Ayanian *et al.*, "Controlling a team of robots with a single input," in *Proc. IEEE ICRA*, 2014, pp. 1755–1762.

[12] G. Podevijn *et al.*, "Gesturing at subswarms: Towards direct human control of robot swarms," in *Towards Autonomous Robotic Systems*. Springer, 2014, pp. 390–403.

[13] T. Setter *et al.*, "Haptic interactions with multi-robot swarms using manipulability," *Journal of Human-Robot Interaction*, vol. 4, no. 1, pp. 60–74, 2015.

[14] S. Erhart and S. Hirche, "Model and analysis of the interaction dynamics in cooperative manipulation tasks," *IEEE Transactions on Robotics*, 2016.

[15] W. Kim *et al.*, "A comparison of position and rate control for telemanipulations with consideration of manipulator system dynamics," *IEEE Transactions on Robotics and Automation*, vol. 3, no. 5, pp. 426–436, October 1987.

[16] K.-H. Jo and J. Lee, "Multi-robot cooperative localization with optimally fused information of odometer and gps," in *Proc. ICCAS*, 2007, pp. 601–605.

[17] K.-S. Chang *et al.*, "The augmented object model: Cooperative manipulation and parallel mechanism dynamics," in *Proc. IEEE ICRA*, vol. 1, 2000, pp. 470–475.

[18] P. Song and V. Kumar, "A potential field based approach to multi-robot manipulation," in *Proc. IEEE ICRA*, vol. 2, 2002, pp. 1217–1222.

[19] G. A. Pereira *et al.*, "Decentralized algorithms for multi-robot manipulation via caging," *International Journal of Robotics Research*, vol. 23, no. 7-8, pp. 783–795, 2004.

[20] T. Wimböck *et al.*, "Comparison of object-level grasp controllers for dynamic dexterous manipulation," *International Journal of Robotics Research*, vol. 31, no. 1, pp. 3–23, 2012.

[21] D. Williams and O. Khatib, "The virtual linkage: A model for internal forces in multi-grasp manipulation," in *Proc. IEEE ICRA*, 1993, pp. 1025–1030.

[22] D. Sieber *et al.*, "Multi-robot manipulation controlled by a human with haptic feedback," in *Proc. IEEE/RSJ IROS*, 2015.

[23] N. Hogan, "Impedance control: An approach to manipulation: Part iiimplementation," *Journal of Dynamic Systems, Measurement, and Control*, vol. 107, no. 1, pp. 8–16, 1985.

[24] H. K. Khalil and J. Grizzle, *Nonlinear systems*. Prentice hall New Jersey, 1996, vol. 3.

[25] F. E. Udwadia and R. E. Kalaba, "A new perspective on constrained motion," *Proceedings: Mathematical and Physical Sciences*, pp. 407–410, 1992.

[26] J. B. Kuipers, *Quaternions and rotation sequences*. Princeton university press Princeton, 1999, vol. 66.

[27] M. Ji and M. B. Egerstedt, "Distributed coordination control of multiagent systems while preserving connectedness." 2007.

[28] K.-K. Oh *et al.*, "A survey of multi-agent formation control," *Automatica*, 2014.

[29] C. I. Aldana *et al.*, "Pose consensus in networks of heterogeneous robots with variable time delays," *International Journal of Robust and Nonlinear Control*, 2014.

[30] C. D. Godsil *et al.*, *Algebraic graph theory*. Springer New York, 2001.

[31] M. Mesbahi and M. Egerstedt, *Graph theoretic methods in multiagent networks*. Princeton University Press, 2010.

[32] O. Khatib, "Real-time obstacle avoidance for manipulators and mobile robots," *The International Journal of Robotics Research*, vol. 5, no. 1, pp. 90–98, 1986.

[33] M. I. García Planas *et al.*, "Sufficient conditions for controllability and observability of serial and parallel concatenated linear systems," 2014.

Dominik Sieber received his Diplom degree in Electrical and Computer Engineering from the Technical University of Munich, Munich, Germany in 2011 and is currently working towards a Doctor of Engineering degree in Electrical and Computer Engineering at the Chair of Information-oriented Control, Department of Electrical and Computer Engineering, Technical University of Munich (TUM), Germany. His research interests include human network interaction and cooperative robotic manipulation.

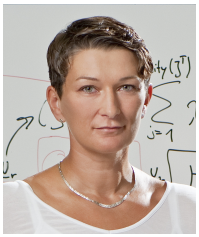

Sandra Hirche (M'03-SM'11) received the Diplom-Ingenieur degree in aeronautical engineering from Technical University Berlin, Germany, in 2002 and the Doktor-Ingenieur degree in electrical engineering from Technical University of Munich, Germany, in 2005. From 2005 to 2007 she was awarded a Postdoc scholarship from the Japanese Society for the Promotion of Science at the Fujita Laboratory, Tokyo Institute of Technology, Japan. From 2008 to 2012 she has been an Associate Professor at Technical University Munich. Since 2013 she is TUM Liesel Beckmann Distinguished Professor and heads the Chair of Information-oriented Control in the Department of Electrical and Computer Engineering at Technical University of Munich. Her main research interests include cooperative, distributed and networked control with applications in human-robot interaction, multi-robot systems, and general robotics.